Multiconfiguration resonating-group theory of the seven-nucleon system with realistic cluster wave functions

Y. Fujiwara
Department of Physics, University of Michigan, Ann Arbor, Michigan 48109

Y. C. Tang
School of Physics and Astronomy, University of Minnesota, Minneapolis, Minnesota 55455

(Received 18 May 1984)

The properties of the seven-nucleon system are examined with a multiconfiguration and multichannel resonating-group calculation. The cluster internal functions employed explain the charge-form-factor data over a wide range of q^2 and satisfy the variational stability condition quite well. The model space used is spanned by $^3H+\alpha$, $n+^6Li$, $n+^6Li^*$, and $d+^5He$ cluster configurations. The result shows that the specific distortion of the $^3H+\alpha$ system is quite significant. With our multiconfiguration calculation, the ground-state energy is improved by more than 1 MeV. The calculated level spectrum agrees well with the level spectrum empirically determined. The energy positions of both natural-parity and unnatural-parity levels are reasonably explained. In addition, we find that, because of centrifugal-barrier effects, the aligned configuration generally makes the most significant contribution. The characteristics of nucleon-exchange terms are also briefly examined. Here it is found that, at sufficiently high energies where sharp resonance levels do not exist, the essential properties of these terms can already be learned by performing relatively simple single-configuration calculations.

I. INTRODUCTION

The resonating-group method[1,2] (RGM) has been utilized, over the past two or three decades, to study level structures and reaction mechanisms in many nuclear systems.[3–5] As is well known, this method is especially suited to investigate the properties of light- and medium-weight nuclei where the formation of nucleon clusters plays an important role. Because of its microscopic nature and resulting computational complexities, however, the progress in this field of cluster physics has not been very rapid. Except for light two-cluster systems consisting of s-shell clusters, existing calculations have frequently been performed with a single cluster configuration and with the constituent clusters described by simple translationally-invariant shell-model wave functions which do not properly account for the density distribution and the nucleon correlation behavior. As a consequence of these simplifications, the results obtained can generally be viewed to have only qualitative, or at most, semiquantitative, significance. A typical example is the microscopic RGM study of the ^{32}S nucleus by Ando *et al.*,[6] where a single $^{16}O+^{16}O$ cluster configuration was adopted, with the ^{16}O nuclei assumed to occupy the lowest configurations in harmonic-oscillator wells. By examining the calculated phase-shift characteristics, these authors obtained interesting information concerning the existence of quasimolecular structures in this medium-weight nucleus. On the other hand, a comparison with the results of Schultheis and Schultheis,[7] using the microscopic α-cluster model in which ^{32}S is described by a more flexible wave function consisting of eight α clusters, does show that the energies of the quasimolecular states calculated by Ando *et al.* are not too reliable.[8] This indicates that, from a quantitative viewpoint, the simplifying assumptions adopted by these latter authors are too drastic and a better calculation, involving more realistic ^{16}O internal wave functions and with specific distortion effects taken into consideration, should be performed.

Extensive RGM studies with multiple cluster configurations have been undertaken by Hackenbroich and his collaborators.[9,10] These are elaborate calculations which required lengthy computing periods. In their consideration of the six-nucleon system,[11] for example, $d+\alpha$, $^3He+^3H$, $p+^5He(\frac{3}{2}^-)$, $n+^5Li(\frac{3}{2}^-)$, $p+^5He^*(\frac{1}{2}^-)$, $n+^5Li^*(\frac{1}{2}^-)$, $p+^5He^{**}(\frac{3}{2}^+)$, and $n+^5Li^{**}(\frac{3}{2}^+)$, configurations were included. For the nucleon-nucleon interaction, they chose to employ a potential possessing a strong repulsive core which necessitates the introduction of Jastrow anticorrelation factors into the trial wave function. To simplify the computation, they were then compelled to adopt a rather crude procedure[12,13] to handle these complicated factors and the kinetic-energy part of the calculation (for details, see Ref. 12 and subsection 5.3c of Ref. 2). This is unfortunate, since their adopted procedure is difficult to comprehend and the resulting uncertainties cannot be readily estimated. Therefore, it is our opinion that the calculations of Hackenbroich and collaborators did yield useful information but should not be quantitatively overemphasized.

In this investigation, we wish to learn the importance of adopting in RGM calculations multiple cluster configurations and realistic cluster internal wave functions. For this purpose, we choose the seven-nucleon system for a careful and systematic study. This particular system is chosen, not only because the computational requirement is less severe due to the relatively small number of nucleons involved, but also because of the following reasons: (i)

even in the low-excitation region, many cluster configurations are involved; (ii) the constituent cluster ^{6}Li is known to exhibit strong nucleon-correlation properties in the form of $d+\alpha$ clustering and its charge-form-factor values have been measured over a wide q^2 range; (iii) for the $^3H+\alpha$ configuration, where the interacting clusters have a small nucleon-number difference, core-exchange effects are very important;[14] (iv) the level structure is rather well established and has been summarized recently by Knox and Lane;[15] and (v) the seven-nucleon system is significant in astrophysical[16] and fusion-reaction[17] applications.

Since we are aiming for a general understanding, we shall strive to include only essential ingredients in the calculation such that the results can be interpreted in an especially simple and clear manner. Thus, we shall perform the present calculation by omitting the Coulomb interaction and by adopting a purely central nucleon-nucleon potential. Because of the long-range nature of the Coulomb force, its effects can be easily estimated. As for noncentral spin-orbit and tensor forces, these are necessary for discussing detailed features but are not essential in light systems if one's desire is mainly to understand the basic behavior of the intricate interplay among various cluster configurations.[18]

Preliminary investigations[19–21] in the seven-nucleon system have been carried out to lay the proper groundwork for the present study. In Ref. 19 (hereafter referred to as FT1), we have performed a calculation with a single $n+^6$Li cluster configuration but a number of different ^{6}Li internal functions. The purpose there was to determine the influence of the clustering and charge-form-factor behavior of ^{6}Li on the properties of the $n+^6$Li system. By examining the cross-section and phase-shift results, it was found that, in the low-energy region, a proper consideration of $d+\alpha$ cluster correlations in ^{6}Li is essential to explain the resonance structure, while in the high-energy region one must adopt in the calculation a ^{6}Li internal function which yields the empirical form-factor values over a wide q^2 range. Next, we performed a calculation, reported in Refs. 20 and 21 (hereafter referred to as FT2 and FT3, respectively), to study channel-coupling effects with multiple cluster configurations. In this latter calculation, to be designated as the shell model-resonating group method (SM-RGM) calculation, we included $^3H+\alpha$, $n+^6$Li, and $n+^6$Li* configurations, but with the simplification of choosing for the ^{3}H, ^{6}Li, and ^{6}Li* clusters lowest-configuration harmonic-oscillator shell-model functions having the same width parameter. The interesting findings there were that the level structure of ^{7}Li, determined by Knox and Lane with a careful R-matrix analysis,[15] can be reasonably explained and that the aligned $n+^6$Li* configuration makes, in general, the most significant contribution because of centrifugal-barrier effects.

In this study, we combine the features incorporated in these preliminary investigations. In other words, we examine channel-coupling effects in a RGM calculation employing flexible ^{3}H and ^{6}Li internal functions which account for cluster correlations and which yield satisfactory values for the charge form factors. As is expected, the resulting calculation turns out to be quite complicated, requiring the formulation of a three-cluster RGM.[22] Recently, however, we have developed for this formulation the necessary analytical technique[22] which includes the extensive use of the method of integral transform. As a consequence, we have found that even such a complicated problem can be solved with reasonable computational periods on moderate-speed computers.

It is appropriate to mention that there also exist other recent investigations in the seven-nucleon system. These are the following: (i) RGM calculations by Beck *et al.*[23] and by Kanada *et al.*[24] These calculations are mainly aimed toward an understanding of the effects of specific distortion in the low-lying states of ^{7}Li. In the study of Beck *et al.*, the cluster configurations included are the two-cluster configuration $^3H+\alpha$ and the three-cluster configurations $n+d(T=0)+\alpha$ and $n+d^*(T=1)+\alpha$, with the $d+\alpha$ and $d^*+\alpha$ subsystems restricted to have relative orbital angular momenta equal to zero. In the investigation carried out by Kanada *et al.*, specific distortion effects are taken into consideration by the introduction of a $^3H^*+\alpha$ configuration to improve the description of the compound nucleus in the strong-interaction region.[25] Both calculations showed that these effects are moderately important and, for the $L=1$ ground state, the energy obtained with specific distortion accounted for is about 0.7 MeV better than that obtained with a single-configuration $^3H+\alpha$ calculation. (ii) RGM calculation by Hofmann *et al.*[26] This is a multichannel calculation including $^3H+\alpha$, $n+^6$Li, $n+^6$Li*, and $d+^5$He cluster configurations. The nucleon-nucleon potential[27] used contains central, spin-orbit, and tensor components. Because of the presence of a strong repulsive core, the above-mentioned crude procedure of Hackenbroich and collaborators has to be adopted again, resulting in some impairment in the quantitative value of this calculation. Even so, however, it is qualitatively useful. Together with our present investigation, we shall show in the following that a rather complete understanding of the main characteristics of the level structure and the reaction mechanism in the seven-nucleon system can now be achieved.

The outline of this paper is as follows. In Sec. II, we give a brief description of the formulation and describe the cluster internal functions. Here, also, we shall discuss some features of the Pauli resonances which generally occur in a microscopic formulation employing antisymmetric wave functions. The results for the calculation with $^3H+\alpha$, $n+^6$Li, and $n+^6$Li* cluster configurations are presented in Sec. III. In Sec. IV, we further enlarge the model space and examine the effects of including also the $d+^5$He configuration in an angular-momentum state where this cluster configuration is expected to have the most significant influence. Finally, in Sec. V, we summarize the findings of this investigation and make some concluding remarks.

II. FORMULATION AND GENERAL DISCUSSION

A. Brief discussion of the formulation

The analytical formulation for a general three-cluster $A+B+C$ system, composed of an α cluster and two s-

shell clusters [i.e., N, d($T=0$), d*($T=1$), ^{3}H, ^{3}He, or α cluster], is given in a recent report.[22] In this report, we show in detail the mathematical derivation of the three-cluster kernel and discuss its algebraic structure. As is evident, such a general formulation is indispensable for our present study, where the purpose is to examine clustering effects of subsystems and channel-coupling effects simultaneously.

In order to utilize the three-cluster RGM formulation for practical applications, coupled-channel equations, involving two-cluster $(A+B)+C$, $(A+C)+B$, and $A+(B+C)$ configurations, are formulated by choosing appropriate relative-motion functions for the $(A+B)$, $(A+C)$, and $(B+C)$ subsystems according to variational procedures constrained by relevant experimental information. These coupled-channel equations are then solved by a variational technique employing Gaussian-type trial functions.[28] The matrix elements of the RGM kernels with respect to these Gaussian functions can be easily calculated with a new technique, developed specifically for this type of investigation by making use of the transformation theory of the complex-generator-coordinate kernel.[29] In Ref. 22, all these steps are expounded and the readers are referred to this reference for details.

In this study, we apply it to the situation where A, B, and C represent N, d or d*, and α clusters, respectively. With our present three-cluster formulation, there exists the restriction[30] that all constituent clusters have to be described by shell-model functions of the lowest configuration in harmonic-oscillator wells of the same width parameter. For our case, this common width parameter α is most appropriately chosen to be equal to 0.514 fm^{-2}, such that the empirically determined rms matter radius of 1.48 fm for the α particle is correctly reproduced.[31]

The two-cluster configurations included in the calculation are the $^3\mathrm{H}+\alpha$, $\mathrm{n}+{}^6\mathrm{Li}$, $\mathrm{n}+{}^6\mathrm{Li}^*$, and $\mathrm{d}+{}^5\mathrm{He}$ configurations, with ^{6}Li* being the $T=0$ excited state of ^{6}Li having a $\mathrm{d}+\alpha$ cluster structure with relative orbital angular momentum I equal to 2. These will be referred to as cluster configurations 1, 2, 3, and 4, respectively. The $\mathrm{p}+{}^6\mathrm{He}$ configuration will not be considered, since it likely has a small influence in view of the fact that the measured cross section for the ^{4}He(^{3}He,p) reaction leading to the first $T=1$ state of ^{6}Li at 3.56 MeV is very small.[32] As for the $\mathrm{d}^*+{}^5\mathrm{He}$ configuration, we shall also not include it here, because it has a higher energy threshold and, being responsible for the process of four-particle decay, cannot really be properly accounted for with our present formulation. In any case, it is our belief[2] that the Pauli principle has the effect of reducing greatly the differences between seemingly different cluster structures when the nucleons are close to one another; hence, especially in the low-excitation region, it is a good approximation to omit some cluster configurations in order to reduce somewhat the computational effort.

Since the nucleon-nucleon potential adopted is purely central, both the total orbital angular momentum L and the total spin angular momentum S ($S=\frac{1}{2}$ or $\frac{3}{2}$) are good quantum numbers. Therefore, the values of these angular momenta can be used to characterize a particular channel wave function. In addition, for a complete characterization, one must of course also specify the cluster configuration and the relative orbital angular momentum l between the constituent clusters which couples with the internal orbital angular momentum I to yield the desired value of L.

The trial wave function in a particular (L,S) state is written as the linear superposition of various channel wave functions ψ_{jl}^{LS}, with the index j specifying the cluster configuration. These channel wave functions are

$$\psi_{1l}^{LS}=\mathscr{A}\left\{\left[\phi_4\phi_3(I=0)\frac{1}{R_1}f_{1l}^{LS}(R_1)Y_l(\hat{R}_1)\right]_L\times\xi_{1S}Z(\mathbf{R}_{\mathrm{c.m.}})\right\}, \tag{1}$$

$$\psi_{2l}^{LS}=\mathscr{A}\left\{\left[\phi_6(I=0)\frac{1}{R_2}f_{2l}^{LS}(R_2)Y_l(\hat{R}_2)\right]_L\times\xi_{2S}Z(\mathbf{R}_{\mathrm{c.m.}})\right\}, \tag{2}$$

$$\psi_{3l}^{LS}=\mathscr{A}\left\{\left[\phi_6^*(I=2)\frac{1}{R_3}f_{3l}^{LS}(R_3)Y_l(\hat{R}_3)\right]_L\times\xi_{3S}Z(\mathbf{R}_{\mathrm{c.m.}})\right\}, \tag{3}$$

$$\psi_{4l}^{LS}=\mathscr{A}\left\{\left[\phi_2\phi_5(I=1)\frac{1}{R_4}f_{4l}^{LS}(R_4)Y_l(\hat{R}_4)\right]_L\times\xi_{4S}Z(\mathbf{R}_{\mathrm{c.m.}})\right\}, \tag{4}$$

with $\mathscr{A}$ being an antisymmetrization operator, ξ_{jS} being appropriate spin-isospin functions, $Z(\mathbf{R}_{\mathrm{c.m.}})$ being any normalizable function describing the motion of the total c.m., and $\mathbf{R}_j$ representing the intercluster vector separation distances. The normalized functions ϕ_n ($n=2$—6) and ϕ_6^* describe the internal spatial structures of the various constituent clusters, with the subscript n denoting the number of nucleons within the cluster. As is evident, l is equal to L for cluster configurations 1 ($^3\mathrm{H}+\alpha$) and 2 ($\mathrm{n}+{}^6\mathrm{Li}$). On the other hand, for cluster configurations 3 ($\mathrm{n}+{}^6\mathrm{Li}^*$) and 4 ($\mathrm{d}+{}^5\mathrm{He}$), several values of l are allowed for a given value of L.[33] Thus, there are, in general, more channels than cluster configurations. For example, if all four cluster configurations are included in the calculation, then in the state with $(L,S)=(1,\frac{1}{2})$, the number of channels involved is equal to six.

For the purpose of gaining a clear understanding of the features arising from the interplay among various cluster configurations, we perform a series of selected calculations, each in a different model space which is defined according to the cluster configurations included. In Table I, we list the various model spaces considered, with SC, DC, TC, and QC denoting single-configuration, double-configuration, triplet-configuration, and quadruple-configuration calculations, respectively.

The linear variational amplitudes or relative-motion functions f_{jl}^{LS} are obtained by following the usual RGM

TABLE I. Model spaces considered.

Model space	Cluster configurations
Single configuration 1 (SC1)	$^3H + \alpha$
Single configuration 2 (SC2)	$n + {}^6Li$
Double configuration 1 (DC1)	$^3H + \alpha$, $n + {}^6Li$
Double configuration 2 (DC2)	$n + {}^6Li$, $n + {}^6Li^*$
Triple configuration (TC)	$^3H + \alpha$, $n + {}^6Li$, $n + {}^6Li^*$
Quadrupole configuration (QC)	$^3H + \alpha$, $n + {}^6Li$, $n + {}^6Li^*$, $d + {}^5He$

procedure. Since this procedure has already been carefully explained in Refs. 4 and 22, we shall not further describe it here.

The nucleon-nucleon potential employed in this investigation has the same form as that used in FT1, FT2, and FT3. It contains an exchange-mixture parameter u which will be chosen according to experimental data[34] on the $^3H + \alpha$ cluster separation energies in the $\frac{3}{2}^-$ ground and $\frac{1}{2}^-$ first excited states of ^7Li. This particular nucleon-nucleon potential is adopted because it yields a satisfactory description of not only the two-nucleon low-energy scattering data, but also the essential properties of the deuteron, ^3H, ^3He, and α particle.[35]

B. Cluster internal wave functions

1. ^3H wave function

The triton wave function has both $N + d$ and $N + d^*$ components. It has the form

$$\tilde{\phi}_3 = N_3 \mathcal{A}[\phi_2 \chi_3(\mathbf{r}_{12}) \tilde{\xi}_3 \tilde{Z}_3(\mathbf{R}_3)] , \quad (5)$$

with N_3 being a normalization factor and $\tilde{Z}_3$ being a function describing the c.m. motion. The spin-isospin function $\tilde{\xi}_3$, appropriate for $(T_3, S_3) = (\frac{1}{2}, \frac{1}{2})$, is chosen to be totally antisymmetric and is given by[36]

$$\tilde{\xi}_3 = \frac{1}{\sqrt{2}}[\xi_{01}(d)\xi_{1/2\,1/2}(N)]_{1/2\,1/2} - \frac{1}{\sqrt{2}}[\xi_{10}(d^*)\xi_{1/2\,1/2}(N)]_{1/2\,1/2} , \quad (6)$$

where the subscripts on the various quantities appearing in the right-hand side denote the values of isospin and spin. With this particular choice for $\tilde{\xi}_3$, the triton function $\tilde{\phi}_3$ has then the property of being totally space symmetric.

The relative-motion function χ_3 is chosen as

$$\chi_3(\mathbf{r}_{12}) = \exp(-\tfrac{1}{3}\eta_3 \alpha r_{12}^2) + c_3 \exp(-\tfrac{1}{3}\zeta_3 \alpha r_{12}^2) . \quad (7)$$

The parameters η_3, ζ_3, and c_3 are determined by minimizing the expectation value of the triton Hamiltonian. The results are

$$\eta_3 = 0.24, \quad \zeta_3 = 1.85, \quad c_3 = 0.593 . \quad (8)$$

With these parameters, the calculated energy expectation value E_3 and rms matter radius $\tilde{R}_3$ are as follows:

$$E_3 = -6.045 \text{ MeV}, \quad \tilde{R}_3 = 1.68 \text{ fm} . \quad (9)$$

Here it is noted that, in particular, the calculated value of $\tilde{R}_3$ agrees well with the empirically determined value.[31] This is gratifying, since in a calculation where strong short-range forces are involved, it is important that the sizes of the interacting nuclei must be properly accounted for.

To make certain that the function $\tilde{\phi}_3$ is a reasonable choice, we have further studied the triton problem with a totally space-symmetric function of the form analogous to that given by Eq. (3) of Ref. 35. Using a ten-Gaussian trial function ($N_0 = 10$) with appropriately chosen but fixed nonlinear parameters α_i ranging from 0.1 to 5.16 fm^{-2}, we obtain $E_3 = -6.031$ MeV and $\tilde{R}_3 = 1.69$ fm, which are quite similar to the values given in Eq. (9). Thus, we are of the opinion that the present choice of $\tilde{\phi}_3$ is indeed satisfactory enough for our purposes.

In Fig. 1, we show a comparison between calculated[37] and experimental values of F_{av}^2, with F_{av} defined by Eq. (22) of Ref. 24. From this figure, one sees that there is a satisfactory agreement, indicating again the adequacy of our chosen triton wave function.

2. ^6Li wave function

The ^6Li wave function $\tilde{\phi}_6$ is taken to be the function ϕ_1 of FT1. This particular function is chosen, because it accounts for the nucleon-correlation behavior and yields satisfactory values for the charge form factor over a wide range of q^2. In this function, the $d + \alpha$ relative-motion function is given by

$$\chi_6(\mathbf{r}_{24}) = \exp(-\tfrac{2}{3}\eta_6 \alpha r_{24}^2) + c_6 \exp(-\tfrac{2}{3}\zeta_6 \alpha r_{24}^2) , \quad (10)$$

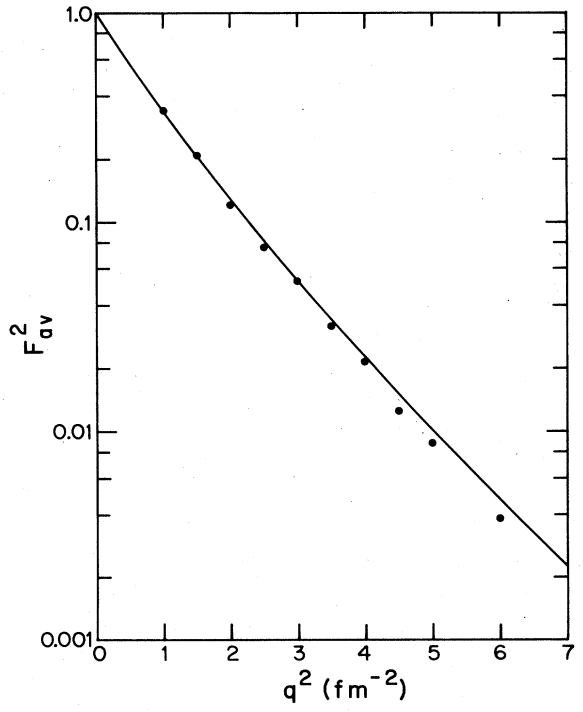

FIG. 1. Square of average charge form factor F_{av} of the three-nucleon system.

with

$$\eta_6=0.0841,\ \zeta_6=0.60,\ c_6=2.337\ . \tag{11}$$

In arriving at these parameter values, we have made a variational calculation with $u=1$, subject to the constraint that the empirical charge-form-factor data be reasonably reproduced (see Fig. 1 of FT1). With this ^{6}Li wave function, the $d+\alpha$ cluster separation energy is calculated to be 2.85 MeV which compares favorably with the empirical value of 2.34 MeV obtained by making a Coulomb correction of 0.86 MeV to the experimental result of 1.48 MeV.[34]

It should be mentioned that, with a strict variational procedure without the charge-form-factor constraint, the optimum cluster separation energy obtained with $u=1$ and a flexible five-Gaussian trial function for χ_6 is 2.99 MeV, which is only 0.14 MeV better than the above-mentioned value. This indicates that our chosen ^{6}Li wave function fulfills, to a satisfactory extent, the variational stability condition which is very important in a calculation utilizing a large model space, as has been emphasized previously by LeMere *et al.*[38] and, more recently, by Kajino *et al.*[39]

The calculated $n+{}^6$Li threshold occurs at 3.15 MeV above the $^3H+\alpha$ threshold. This is in reasonable agreement with the empirical result of 3.92 MeV, obtained by using the measured value of 4.78 MeV (Ref. 34) and a Coulomb correction of 0.86 MeV.

3. $^6Li^*$ wave function

As is well known, ^{6}Li* has predominantly a $d+\alpha$ cluster configuration with relative orbital angular momentum I equal to 2. It is particle unstable, but the lifetime is comparatively long because of the presence of Coulomb and centrifugal barriers. In addition, one should note that, when such a structure occurs in the seven-nucleon system, the extra neutron may have a further stabilizing effect (see the discussion in subsection 3.6b of Ref. 2). Thus, for a description of the influence of this sequential-decay cluster structure $n+{}^6$Li*, it is not unreasonable to adopt a normalized bound-state-type function $\tilde{\phi}^*_6$ for ^{6}Li*, which has a $d+\alpha$ relative-motion function of the form

$$\chi^*_6(\mathbf{r}_{24})=[\exp(-\tfrac{2}{3}\eta^*_6\alpha r^2_{24}) +c^*_6\exp(-\tfrac{2}{3}\zeta^*_6\alpha r^2_{24})]r^2_{24}Y_{2M}(\hat{r}_{24})\ . \tag{12}$$

For the determination of the parameters η^*_6, ζ^*_6, and c^*_6, there is, of course, no simple and well-defined criterion. This is, however, not too serious, since in a calculation with a large model space, the choice of these parameters is not too critical from a variational viewpoint. Only certain essential features have to be reasonably accounted for and these features are the clustering property and the excitation energy of ^{6}Li*. Thus, we simply choose η^*_6 and ζ^*_6 as equal to η_6 and ζ_6, respectively, and variationally determine c^*_6. The result with $u=1$ is

$$c^*_6=0.719\ . \tag{13}$$

With these parameters, the excitation energy of ^{6}Li* is calculated to be 4.58 MeV, which is not too different from the empirical value of 3.60 MeV, obtained by averaging the measured excitation energies[34] of the low-excited $^3D_3$ and $^3D_2$ states according to spin-orbit weighting.

4. ^{5}He wave function

The above-mentioned discussion is also applicable to the case of ^{5}He, having predominantly a $n+\alpha$ cluster configuration with relative orbital angular momentum $I=1$. Therefore, we choose for its description a normalized function $\tilde{\phi}_5$, which has a $n+\alpha$ relative-motion function χ_5 given by

$$\chi_5(\mathbf{r}_{14})=[\exp(-\tfrac{2}{5}\eta_5\alpha r^2_{14}) +c_5\exp(-\tfrac{2}{5}\zeta_5\alpha r^2_{14})]r_{14}Y_{1M}(\hat{r}_{14})\ . \tag{14}$$

In this case, the determination of the parameters η_5, ζ_5, and c_5 is again not clear-cut. The main criterion which we adopted was that the $n+\alpha$ cluster separation energy should turn out to be -2.22 MeV, a value obtained by utilizing experimental information for the $^2P_{3/2}$ and $^2P_{1/2}$ states. With this criterion, we found sets of (η_5,ζ_5) values, together with the corresponding values of c_5 determined variationally. By further demanding that ^{5}He should possess strong clustering property, we finally decided to use

$$\eta_5=0.20,\ \zeta_5=0.84,\ c_5=0.344\ . \tag{15}$$

The important point to note here is that η_5 is appreciably smaller than 1, indicating clearly[40] that our adopted function $\tilde{\phi}_5$ does describe ^{5}He as having a considerable degree of $n+\alpha$ clustering.

By also using calculated energy expectation values of the deuteron and the α particle, the $d+{}^5$He threshold is found to be at 8.23 MeV above the $^3H+\alpha$ threshold. This is again a reasonable result, since the empirical value after Coulomb correction is equal to 8.47 MeV.

5. Important features of cluster internal wave functions

The essential point we wish to stress is about the variational stability condition. In our present study, where the main concern is on the bound-state and phase-shift properties of $^3H+\alpha$ and $n+{}^6$Li systems, it is important that the wave functions describing these stable clusters should satisfy this condition. This is so, since the purpose of enlarging the model space is to achieve a realistic account of specific-distortion or channel-coupling effects, rather than to compensate crudely and improperly for the unsatisfactory choice of cluster internal wave functions.

As has been discussed already, our ^{3}H and ^{6}Li wave functions do satisfy quite well the stability condition. For the α particle, our present formulation requires that it be represented by a translationally-invariant shell-model function of $(1s)^4$ configuration in a harmonic-oscillator well of width parameter α, which is chosen to be 0.514 fm^{-2} in order to yield correctly the empirically determined rms matter radius. At first, one might think that such a wave function is too simple. However, we should

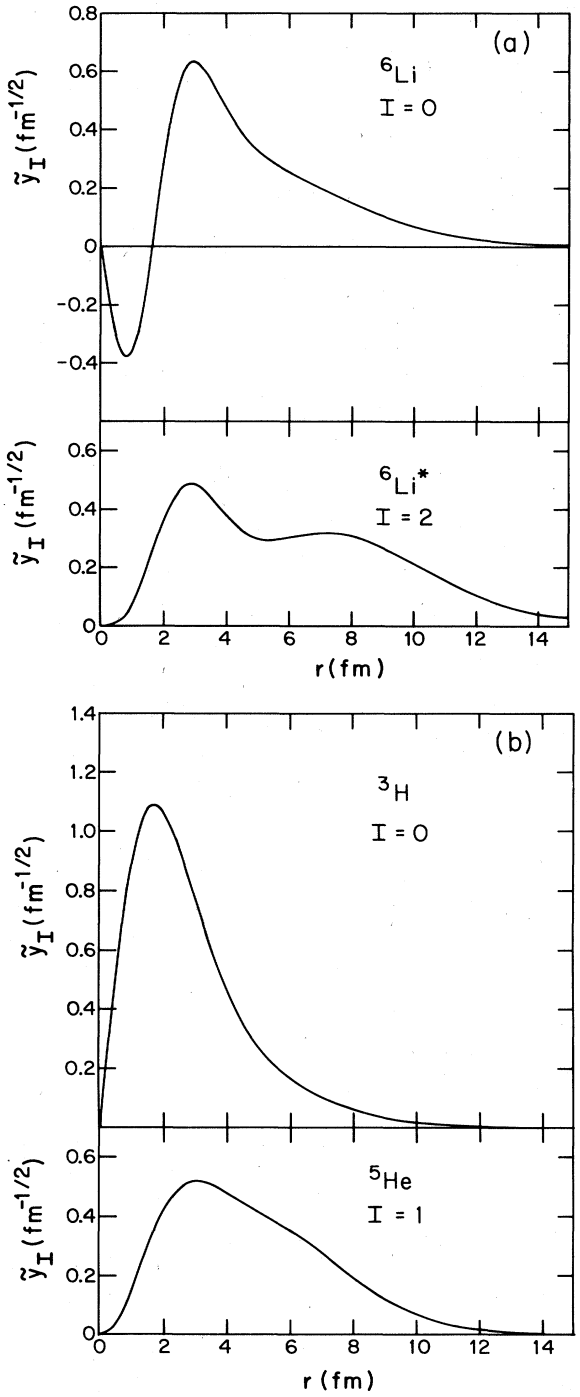

FIG. 2. (a) Reduced-width amplitudes for d + α clustering in ^{6}Li and ^{6}Li*. (b) Reduced-width amplitudes for N + d and N + d* clustering in ^{3}H, and for n + α clustering in ^{5}He.

mention that, because of the compact nature of the α particle, the stability condition is in fact not seriously violated. With this α-particle wave function, the calculated energy expectation value is -24.71 MeV (-23.88 MeV with Coulomb interaction taken into account), which is not greatly different from the value of -25.61 MeV obtained with a flexible trial function consisting of ten Gaussian functions.[35]

In Figs. 2(a) and (b), we show the reduced width amplitudes,[41] defined as

$$\tilde{\mathcal{Y}}_I(r)=[\binom{6}{2}]^{1/2}\left\langle\phi_2\phi_4\frac{1}{r_{24}}\delta(r_{24}-r)Y_{I0}(\hat{r}_{24})\tilde{\xi}_6\tilde{Z}_6\,\middle|\,\tilde{\phi}_6\right\rangle \tag{16}$$

for ^{6}Li ($I=0$), and analogously for other clusters involved. As is discussed in FT1, where the properties of a number of suitably chosen ^{6}Li wave functions were compared, the fact that $\tilde{\mathcal{Y}}_0$ for ^{6}Li has an appreciable magnitude in the region of large separation distance r is a clear indication that ^{6}Li possesses a large degree of d + α clustering. Based on this knowledge, one can similarly conclude by examining the behavior of the reduced width amplitudes in the ^{5}He and ^{6}Li* cases that our chosen wave functions also describe quite well the strong clustering properties of these two nuclei.

C. S-matrix elements

By solving coupled integro-differential equations, we obtain the relative-motion functions f_{jl}^{LS} and, hence, the S-matrix elements S_{fi}^L in $S=\frac{1}{2}$ and $\frac{3}{2}$ states. In the following discussion, we shall be mainly concerned with an examination of the properties of these matrix elements.

As in FT2 and FT3, we shall label the initial channel i or the final channel f not by the type of cluster configuration and the value of the orbital angular momentum l, but by the following convenient convention. If the channel index i or f is represented by a single number, the ^{3}H + α cluster configuration is referred to and this single number represents the value of l between the ^{3}H and α clusters. On the other hand, if the channel index is represented by a double number, then the n + ^{6}Li, n + ^{6}Li*, or d + ^{5}He cluster configuration is referred to, with the first and second numbers denoting the values of l and I, respectively.[42] For example, in the $L=1$ state, $S_{32,1}^1$ denotes an off-diagonal element describing the coupling between the ^{3}H + α configuration with $l=1$ and the n + ^{6}Li* configuration with $l=3$, while $S_{21,10}^1$ denotes an off-diagonal element describing the coupling between the n + ^{6}Li configuration with $l=1$ and the d + ^{5}He configuration with $l=2$.

As is customary, the diagonal element will be parametrized in terms of the reflection coefficient η_{ii}^L and the phase shift δ_{ii}^L, i.e.,

$$S_{ii}^L=\eta_{ii}^L\exp(2i\delta_{ii}^L)\ . \tag{17}$$

For the coupling or off-diagonal element S_{fi}^L, we shall mainly be interested in its absolute value, namely, the transmission coefficient given by

$$\eta_{fi}^L=|S_{fi}^L|\ . \tag{18}$$

D. Brief discussion of Pauli resonances

It is well known[4] that, with a microscopic formulation utilizing totally antisymmetric wave functions, Pauli resonances (also called almost-forbidden states in the litera-

TABLE II. Natural-parity forbidden states in the SM-RGM case. The SU_3 states labeled $(30)_1$, $(30)_2$, and $(11)_1$ are FS composed of linear combinations of different cluster configurations.

S	L	Number of FS in QC model space	Cluster configuration $^3H + \alpha$	$n + {}^6Li(20)$ $[(n + {}^6Li) + (n + {}^6Li^*)]$	$d + {}^5He$
	0	4	(00),(20)	(20)	(20)
$\frac{1}{2}$	1	5	(10)	$(30)_1$	$(10),(30)_2,(11)_1$
	2	3	(20)	(20)	(20)
	3	2		$(30)_1$	$(30)_2$
	0	2		(20)	(20)
$\frac{3}{2}$	1	4		(30)	$(10),(30),(11)_1$
	2	2		(20)	(20)
	3	2		(30)	(30)

ture[43]) with definite characteristic energies will be present. In a preliminary study[44] of the seven-nucleon system employing the present three-cluster RGM formalism, these resonances were found to occur in the higher-excitation region and have the interesting property of indirectly enhancing the coupling between various cluster configurations. In this subsection, we shall briefly consider the question concerning the number of such resonances in a definite (L,S) state and demonstrate their presence in two calculations adopting different model spaces.

For our purpose, it is useful to consider first the SM-RGM case where all clusters involved are described by shell-model functions of the lowest configuration in harmonic-oscillator wells having a common width parameter. In this case, the well-known feature in a single-configuration formulation is that there exist redundant or forbidden states (FS) which are states with zero eigenvalue for the normalization kernel. If one expands the model space to include multiple cluster configurations, then extra FS will appear as a result of the coupling among the various configurations. Thus, one expects that the number of FS will become quite large when a large model space is adopted. This is shown in Table II, where all FS are classified according to the $(\lambda\mu)$ label of the SU_3 irreducible representation and have natural parity $\pi=(-1)^L$. In addition, we use the convention to denote those FS which are already present in the single-configuration case by $(\lambda\mu)$ with no suffix, and to denote the additional FS which arise from coupling among cluster configurations by $(\lambda\mu)$ with a suffix [i.e., $(30)_1$, $(30)_2$, and $(11)_1$]. For example, if the model space with a single $^3H + \alpha$ configuration is expanded to also include the $n + {}^6Li(20)$ configuration, then one finds from Table II that the number of FS in the $(L,S)=(1,\frac{1}{2})$ state increases from one to two, with the extra one coming from configuration coupling.

In our present investigation where more flexible wave functions are used to describe the ^3H, ^5He, ^6Li, and $^6Li^*$ clusters, FS will no longer exist, but there appear now almost-forbidden states which are eigenstates of the norm operator with near-zero eigenvalues and which are equal in number to the FS in the SM-RGM case. These states have definite characteristic energies and exhibit themselves as steplike or dispersionlike resonances in the phase-shift curves of various incident channels. We shall refer to these resonances as Pauli resonances, since they arise as a consequence of the exact treatment of antisymmetrization.

The existence of Pauli resonances is illustrated in Figs. 3 and 4, where the results obtained with DC1 and DC2 calculations, respectively, are depicted. The exchange-mixture parameter u is taken to be 1. In Fig. 3, we show in the $(L,S)=(0,\frac{1}{2})$ state the phase shift $\delta^0_{00,00}$ and the transmission coefficient $\eta^0_{0,00}$ as a function of E_2, the relative energy of the neutron and ^6Li in the c.m. system. According to Table II, one expects that there should exist three Pauli resonances in this particular (L,S) state.

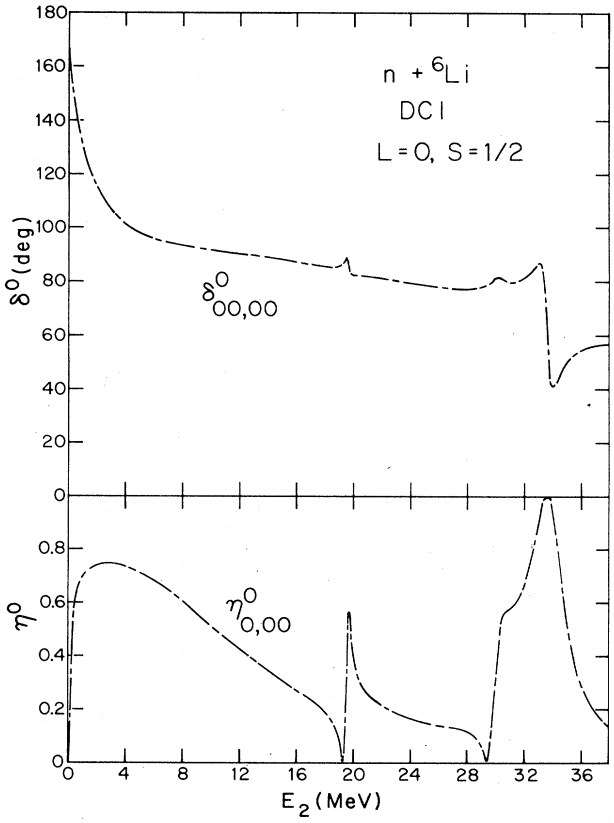

FIG. 3. Pauli resonances in the DC1 calculation with $(L,S)=(0,\frac{1}{2})$.

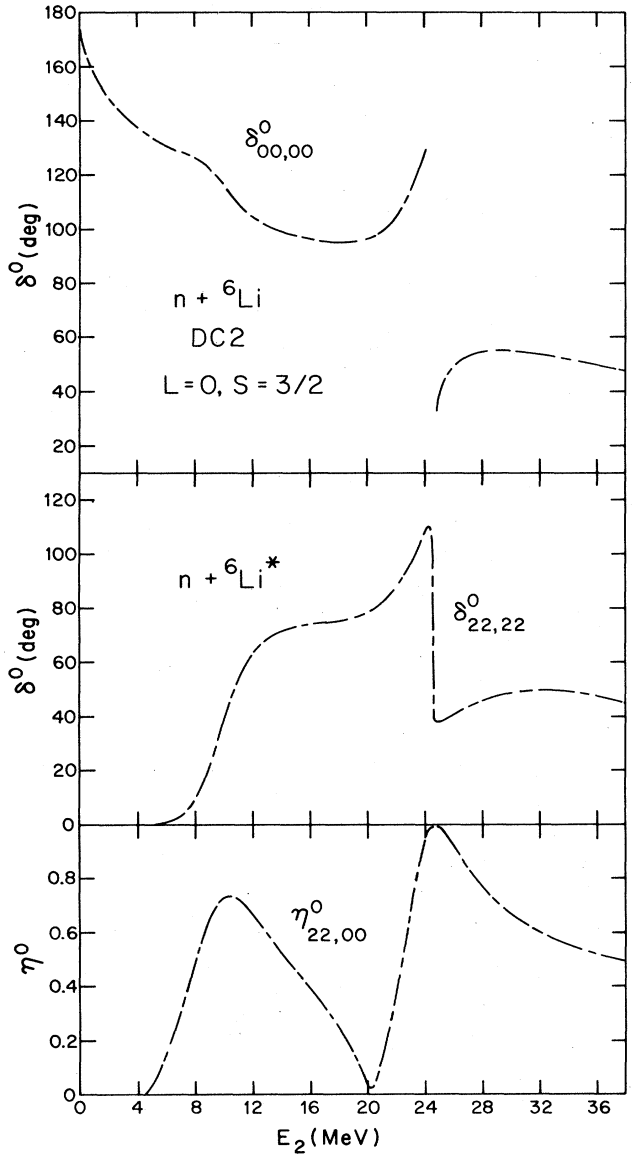

FIG. 4. Resonance structures in the DC2 calculation with $(L,S)=(0,\frac{3}{2})$.

From Fig. 3, it is indeed seen that three dispersionlike resonances do appear, with the lowest one occurring at E_2 equal to 19.7 MeV.

In Fig. 4 we show, in the $(L,S)=(0,\frac{3}{2})$ state the n + ^{6}Li phase shift $\delta^0_{00,00}$, the n + ^{6}Li* phase shift $\delta^0_{22,22}$, and the transmission coefficient $\eta^0_{22,00}$ as a function of E_2. Here one notes that there appear two resonances,[45] with the higher-energy one at 24.6 MeV being predominantly a Pauli resonance and the lower-energy one at 10.5 MeV being predominantly a potential resonance[2] having a n + ^{6}Li* cluster structure with $l=2$. As will be discussed in Sec. III, this latter resonance has, in particular, a rather significant influence on the phase-shift behavior of the n + ^{6}Li channel in the low-energy region.

Pauli resonances of correct number are also found in other (L,S) states. In general, these resonances appear at energies higher than about 20 MeV. In the energy region where they occur, the coupling among various cluster configurations becomes generally rather strong, and the behavior of the seven-nucleon system is quite complicated.

It should be stressed that, within the adopted model space, the Pauli resonance is a real resonance which should be treated in the same footing as any other type of resonance.[46,47] On the other hand, one should also note that its characteristics are rather sensitively dependent upon the model space used. For example, even the introduction of a small imaginary potential into the RGM formulation will affect its behavior in a rather significant manner.[48] Thus, for the sake of achieving a simple and clear understanding of the level structure and the reaction mechanism, we shall restrict ourselves mainly to low energies below 20 MeV, at which the effect of Pauli resonances is expected to be substantially reduced.

III. RESULTS OF CALCULATIONS IN SC, DC, AND TC MODEL SPACES

A. Introductory remarks

It is well known[2] that the Pauli principle has the important effect of substantially reducing the differences between apparently different nonorthogonal wave functions. This has the practical consequence that, especially at low excitation energies, one can frequently learn the essential characteristics of a nuclear system by employing a trial function which consists of a relatively small number of wave functions in different cluster representations. In this investigation, we shall make use of this fact to reduce the computational periods by performing the calculation in two distinct steps. In the first step, we stay within the SC, DC, and TC model spaces and make a detailed comparison of the results obtained when the model space is systematically enlarged. Then, as the second step, we proceed into the QC model space by adding the d + ^{5}He cluster configuration, but carry out the investigation only in a selected $(L,S)=(1,\frac{1}{2})$ state where the addition of this particular cluster configuration is expected to be most significant. The purpose of this latter step is, of course, to see whether a further enlargement of the model space can cause any major modification in the understanding which we gained from the detailed examination performed in the first step.

The results from the first step will be presented exclusively in this section. Then, in the next section (Sec. IV), we discuss the consequences of going into the QC space.

B. Determination of the exchange-mixture parameter and channel coupling effects in states of the ground-state rotational band

The exchange-mixture parameter u in the nucleon-nucleon potential is determined by the criterion that the calculated ^{3}H + α cluster separation energy in the lowest $(L,S)=(1,\frac{1}{2})$ state be nearly equal to 3.17 MeV. As was discussed in FT2, this particular value is obtained by making Coulomb and spin-orbit corrections to the experi-

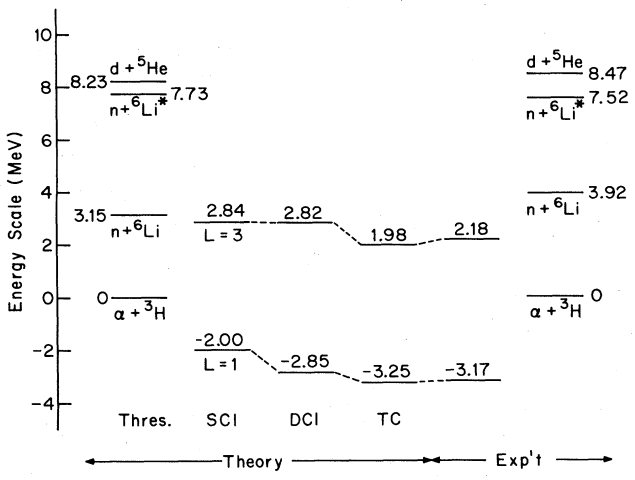

FIG. 5. Comparison of $(L,S)=(1,\frac{1}{2})$ ground-state energies and $(L,S)=(3,\frac{1}{2})$ resonance-state energies obtained with single-configuration SC1, double-configuration DC1, and triple-configuration TC calculations. Calculated and experimental threshold energies for the various cluster configurations are also shown.

mentally determined $^3H+\alpha$ cluster separation energies in the $\frac{3}{2}^-$ ground and the $\frac{1}{2}^-$ first excited states.[34] With $u=1$, we find that the TC calculation yields a value of 3.25 MeV for this energy. Therefore, unless otherwise stated, this value of u will be adopted in all our subsequent calculations.

The ground-state rotational band consists of a $L=1$ bound state and a $L=3$ resonance state. In Fig. 5, we show the improvement of the $^3H+\alpha$ relative energies in these states as one progresses from the SC1 to the DC1 and finally to the TC calculation. From this figure, one notes the following important points:

(i) Specific-distortion or channel-coupling effects lead to an improvement of 1.25 and 0.86 MeV in the $L=1$ and 3 states, respectively. These values are larger than the corresponding values of 0.68 and 0.72 MeV obtained in FT2. This indicates that a careful consideration of the clustering properties of ^{6}Li and ^{6}Li* is quantitatively important.

(ii) In the $L=1$ state, both $n+{}^6$Li and $n+{}^6$Li* cluster configurations seem to be important. This is in contrast to the $L=3$ case, where the improvement comes mainly from the coupling of the $n+{}^6$Li* configuration to the dominant $^3H+\alpha$ configuration. The reason for this has already been discussed in FT2; it is related to the fact that, because of centrifugal-barrier effects, the $n+{}^6$Li* aligned configuration (i.e., $l=L-2$) makes a particularly important contribution.

The agreement between calculated and empirical results is quite satisfactory. In the TC calculation, the level spacing between the $L=1$ and 3 states is 5.23 MeV, which is only about 2% different from the empirical value of 5.35 MeV.

In our calculation, where Coulomb effects are not included, there is some overestimate of the importance of specific distortion. To obtain some idea about what this overestimate may be, we have made a further computation using $u=0.96$. With this u value, the $^3H+\alpha$ cluster separation energies in the $L=1$ state turn out to be 1.48, 2.26, and 2.61 MeV in the SC1, DC1, and TC calculations, respectively. Upon further extrapolating to a TC value of 2.31 MeV (see Fig. 1 of FT2), we find then that the improvement in the ground-state energy is equal to about 1.07 MeV. This is somewhat, but not greatly, smaller than the value of 1.25 MeV already mentioned, suggesting that the omission of Coulomb effects is a reasonable simplification in an investigation where the main purpose is to achieve a general understanding of the essential properties of the seven-nucleon system.

The specific distortion effect of 1.07 MeV obtained here is larger than that of 0.76 MeV obtained in the calculation by Kanada *et al.*,[24] where the breathing-excitation mode of the ^3H cluster is carefully taken into account. This indicates that, although a proper consideration of the breathing mode is certainly of importance, other excitation modes must also be included if a quantitatively reliable estimate of the specific distortion effect is to be obtained.

C. Phase-shift and transmission-coefficient results in $S=\frac{1}{2}$ natural-parity states

In Figs. 6–9, we show the results for the $^3H+\alpha$ phase shifts and transmission coefficients as a function of E_1; the relative energy of the ^3H and the α clusters in the c.m. system; and the $n+{}^6$Li phase shifts and transmission coefficients as a function of E_2, the relative energy of the neutron, and the ^{6}Li cluster in the c.m. system. For the phase shifts, the values obtained in the SC1 or SC2 (dashed curves), DC1 or DC2 (solid circles), and TC (solid curves) cases are shown, while for the transmission coefficients only the values obtained in the TC case are depicted. Also, for clarity in presentation, we shall not show the transmission coefficient for transition into any weakly coupled state where its value is smaller than 0.1 in the whole range of relative energy considered (i.e., 0–20 MeV).

The important features in the various L states will be discussed in the following. In these discussions, we shall frequently refer to the findings from the SM-RGM calculations of FT2 and FT3.

1. $L=0$ state [Figs. 6(a) and (b)]

From Fig. 6(a), one notes, as in FT2, the appearance of cusps[49] at the $n+{}^6$Li threshold and the predominance of coupling between $^3H+\alpha$ and $n+{}^6$Li configurations. These features have already been explained in FT2 and, hence, will not be discussed here further.

The features exhibited by the phase-shift and transmission-coefficient curves in the $n+{}^6$Li channel [Fig. 6(b)] are more complicated, but may be summarized as follows:

(a) Pauli resonances (shown as breaks in the curves) occur at E_2 equal to about 12 and 11.5 MeV in the SC2 and DC2 calculations, respectively. In the TC calcula-

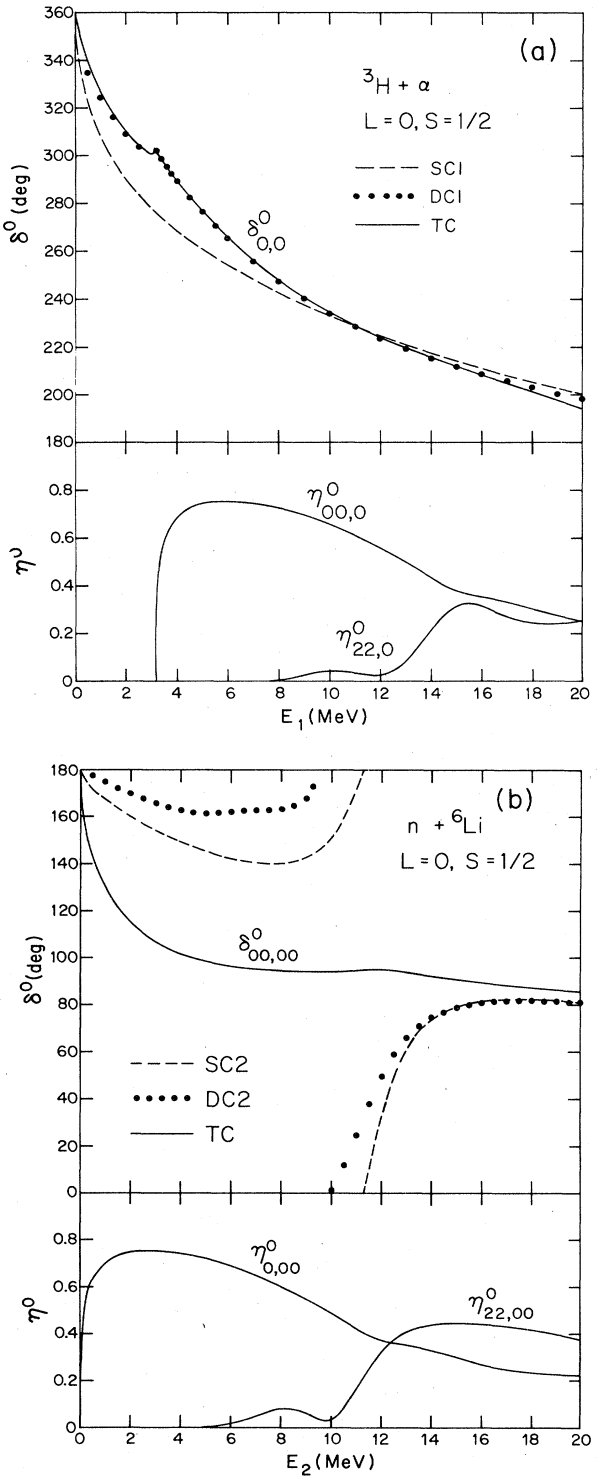

FIG. 6. (a) Calculated phase shifts and transmission coefficients for $(L,S)=(0,\frac{1}{2})$ in the $^3H + \alpha$ channel. The dashed curve, solid circles, and solid curve represent results obtained with SC1, DC1, and TC calculations, respectively. (b) Calculated phase shifts and transmission coefficients for $(L,S)=(0,\frac{1}{2})$ in the n + ^{6}Li channel. The dashed curve, solid circles, and solid curve represent results obtained with SC2, DC2, and TC calculations, respectively.

tion, resonances of this type appear in the higher-energy region above 20 MeV.

(b) The wavy or dispersionlike behavior at around 8 MeV in the DC2 case arises as a consequence of coupling to the $l=2$ potential resonance of n + ^{6}Li* cluster configuration.

(c) With the inclusion of the $^3H + \alpha$ configuration (TC model space), the n + ^{6}Li phase-shift curve becomes very flat when E_2 is between about 5 and 12 MeV. In addition, it is noted that the transmission coefficient $\eta^0_{0,00}$ has a large magnitude in this energy region. These observations indicate that the assumption of a broad $\frac{1}{2}^+$ state, having a predominantly $^3H + \alpha$ and n + ^{6}Li cluster structure, by Knox and Lane[15] in their R-matrix study of the seven-nucleon system is quite reasonable.

(d) In the TC phase-shift curve, the wavy behavior around 14 MeV is due to the interplay of all three cluster configurations, with the n + ^{6}Li*, $l=2$ potential resonance making an important contribution.

Using the phase-shift values at very low energies, one can determine the n + ^{6}Li, S-wave scattering length a_-. The result from the TC calculation is $a_- = 4.71$ fm, which compares favorably with the empirical value of 3.88 fm determined by Knox and Lane.[15]

2. *L=1 state [Figs. 7(a) and (b)]*

The effect of enlarging the model space can be seen quite clearly in this (L,S) state. In Sec. III B, we have discussed the improvement in the ground-state energy as the model space is enlarged from SC1 to DC1 and, finally, to TC. Here, we shall make a similar discussion but with the succession of model spaces being SC2, DC2, and TC.

In the SC2 case, there appears a n + ^{6}Li bound state at E_2 equal to -2.09 MeV and the phase-shift curve shows a smooth, monotonically decreasing behavior [see Fig. 7(b)]. By adding the n + ^{6}Li* cluster configuration to go into the DC2 model space, we find that this bound state is now lowered to -4.74 MeV. In addition, the n + ^{6}Li phase-shift result exhibits the presence of a resonance state at around 6 MeV. This latter state has a dispersionlike behavior, indicating that it has predominantly a n + ^{6}Li* cluster structure. With the further addition of the $^3H + \alpha$ cluster configuration (TC case), a bound state and a resonance state exist at -6.40 and 8 MeV, respectively. For the resonance state, the n + ^{6}Li phase shift shows a steplike behavior, while the $^3H + \alpha$ phase shift shows a dispersionlike behavior. This indicates that this particular resonance state has mainly a n + ^{6}Li structure; however, it contains also a considerable degree of n + ^{6}Li* ($l=1$) and $^3H + \alpha$ clustering, as is evidenced by the large magnitudes of the transmission coefficients $\eta^1_{12,10}$ and $\eta^1_{1,10}$.

That the above-mentioned resonance state at 8 MeV has an appreciable degree of n + ^{6}Li* clustering can also be seen in the following way. In the DC1 calculation, where the n + ^{6}Li* configuration is not included, one notes from Fig. 7(a) that the dispersionlike structure shifts to a much higher energy of about 13 MeV. This indicates indirectly then that the n + ^{6}Li* configuration does contribute significantly in this resonance state.

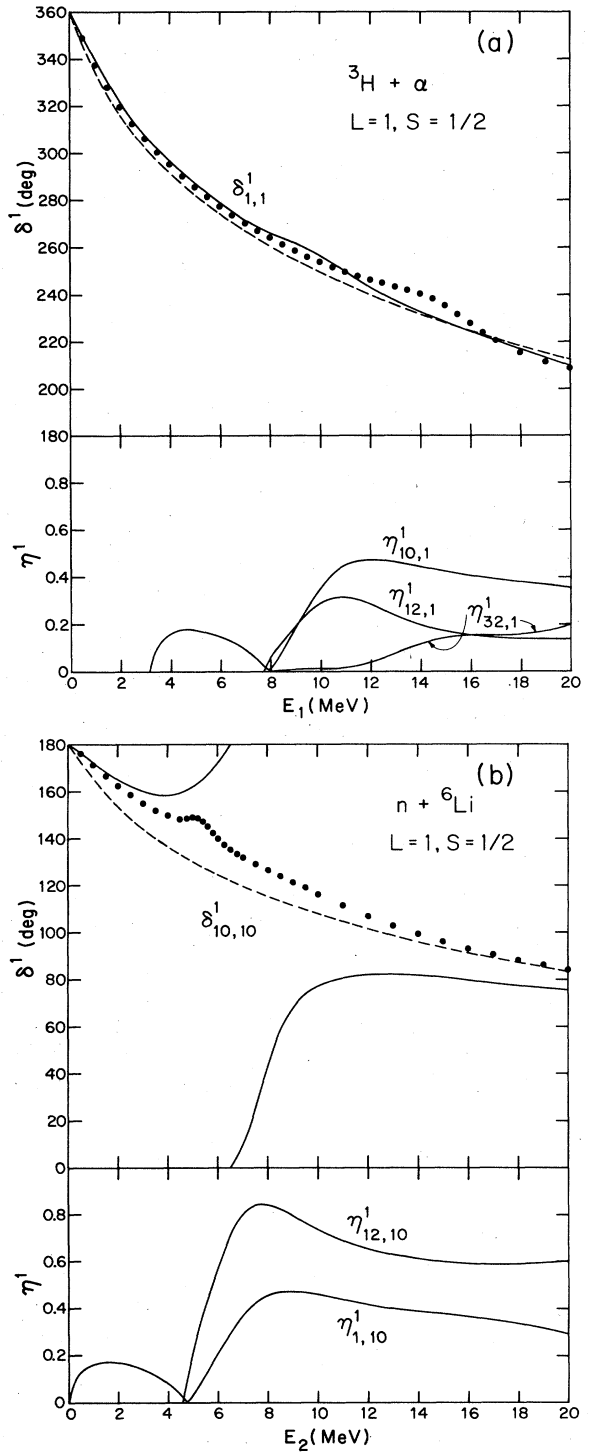

FIG. 7. (a) Same as Fig. 6(a), except that $(L,S)=(1,\frac{1}{2})$. (b) Same as Fig. 6(b), except that $(L,S)=(1,\frac{1}{2})$.

In the TC calculation, the resonance state occurs at about 3.5 MeV above the n + ^{6}Li* threshold. This is in contrast to the findings reported in FT2 and FT3 where the d + α clustering behavior of ^{6}Li and ^{6}Li* is not properly accounted for. There it was found that a resonance state of similar nature does exist, but is located close to the n + ^{6}Li* threshold. Therefore, this investigation shows that, for a quantitative description of the seven-nucleon system, carefully chosen cluster internal wave functions must be employed.

With the further addition of the d + ^{5}He cluster configuration (see Sec. IV) and by making a spin-orbit correction of about 1 MeV, we anticipate that a $\frac{3}{2}^-$ state of $(L,S)=(1,\frac{1}{2})$ will appear at about 6 MeV above the n + ^{6}Li threshold. This is in reasonable agreement with the result of a *R*-matrix study in which such a state with a relatively high excitation is also found to be required.

3. *L*=2 state [Figs. 8(a) and (b)]

From the ^{3}H + α phase-shift curves, it is seen that the n + ^{6}Li* cluster configuration has a larger effect than the n + ^{6}Li cluster configuration. This is quite clearly a consequence of the fact that the relative orbital angular momentum *l* can take on the value 0 in the former configuration but is equal to 2 in the latter configuration. With all three configurations taken into account, one notes that the ^{3}H + α phase shift becomes even slightly positive in

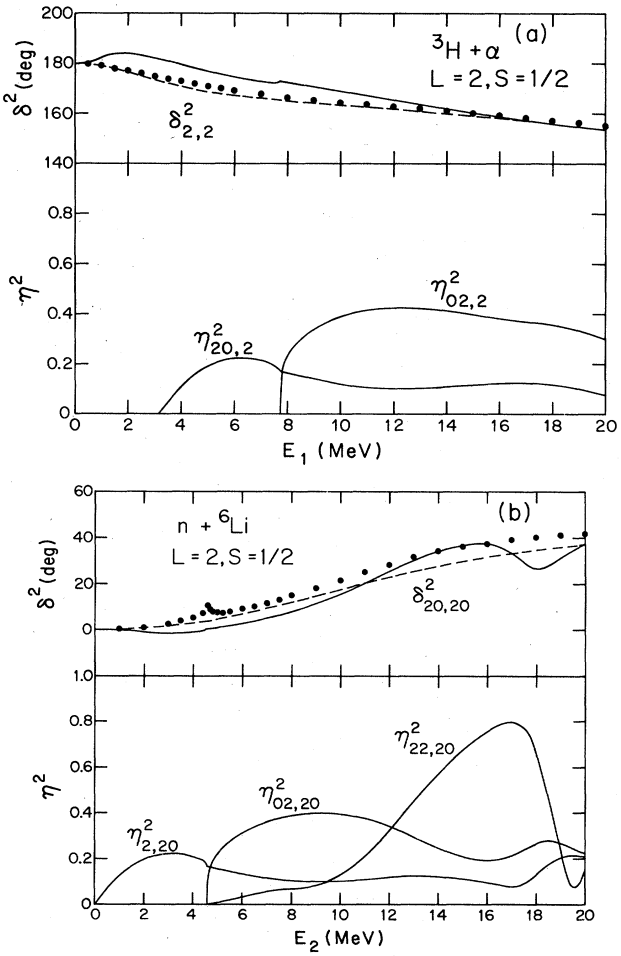

FIG. 8. (a) Same as Fig. 6(a), except that $(L,S)=(2,\frac{1}{2})$. (b) Same as Fig. 6(b), except that $(L,S)=(2,\frac{1}{2})$.

the low-energy region, a finding which has also been reported by Hofmann *et al.*[26]

As expected, a cusp appears in the $^3H + \alpha$, TC phase-shift curve, due to the coupling between the $^3H + \alpha$ channel and the $n + {}^6Li^*$ channel with $l=0$. This cusp is, however, not too prominent and would be difficult to observe experimentallv.

In the $n + {}^6Li$ case [Fig. 8(b)], cusps appear in both the DC2 and TC phase-shift curves. However, the magnitudes of these cusps are quite different, indicating that the inclusion of the $^3H + \alpha$ cluster configuration has a significant effect. In addition, it is seen that the TC phase-shift result shows a dispersionlike resonance behavior at 17.0 MeV. By examining the structure of the $\eta^2_{22,20}$ curve, one can attribute the presence of this resonance to the coupling between the $n + {}^6Li$ configuration and the $n + {}^6Li^*$, $l=2$ resonance. In this respect, we should point out one interesting feature. Such a resonance shows up clearly in the TC case, but not in the DC2 case. This may be a demonstration of the $^3H + \alpha$ doorway effect, which has also been observed in a previous investigation.[44]

From Fig. 8(b), one further notes that, at low energies below 10 MeV, $\eta^2_{02,20}$ is appreciably larger than $\eta^2_{22,20}$. Thus, similar to the finding reported in FT2 and FT3, we also find here that the aligned configuration (i.e., $l=L-2$) of the $n + {}^6Li^*$ structure makes generally the most significant contribution in the low-energy region.

4. *L=3 state [Figs. 9(a) and (b)]*

The most important feature in the $^3H + \alpha$ phase-shift curve is the existence of a sharp resonance state. As has already been discussed in Sec. III B, the effect of channel coupling is quite important here. In the SC1 and TC cases, the resonance energies are, respectively, equal to 2.84 and 1.98 MeV, with the lowering in energy resulting almost entirely from the addition of the $n + {}^6Li^*$, $l=1$ configuration.

The similarity in the SC2 and DC2 results shown in Fig. 9(b) indicates that the direct coupling between the $n + {}^6Li$ and $n + {}^6Li^*$ configurations is quite weak. On the other hand, it is also seen that the inclusion of the $^3H + \alpha$ configuration does yield a fairly significant change in the phase-shift values.

From the transmission-coefficient curves shown in both Figs. 9(a) and (b), one finds again that, at low energies, the aligned configuration of the $n + {}^6Li^*$ channel makes the dominant contribution.

5. *L=4 and 5 states (not shown)*

Because of the centrifugal-barrier effects, one finds that, as in FT2, the $^3H + \alpha$ phase shifts are somewhat affected by the addition of the $n + {}^6Li^*$ aligned configurations, but very little by the addition of the $n + {}^6Li$ cluster structure.

D. Phase-shift and transmission-coefficient results in $S=\frac{3}{2}$ natural-parity states

In the $S=\frac{3}{2}$ state, the $^3H + \alpha$ configuration does not contribute and, hence, the calculations are performed with only the $n + {}^6Li$ and $n + {}^6Li^*$ configurations. The results for the phase shift and the transmission coefficient are shown in Figs. 10—12. In these figures, the values obtained in the SC2 and DC2 cases are represented by dashed and dot-dashed curves, respectively. The salient features are as follows:

1. *L=0 state (Fig. 10)*

In the SC2 case, there appears a Pauli resonance at about 16 MeV. This resonance is shifted to a higher energy of 24.6 MeV when the $n + {}^6Li^*$ configuration is added into the calculation (DC2 case; see also Fig. 4). In addi-

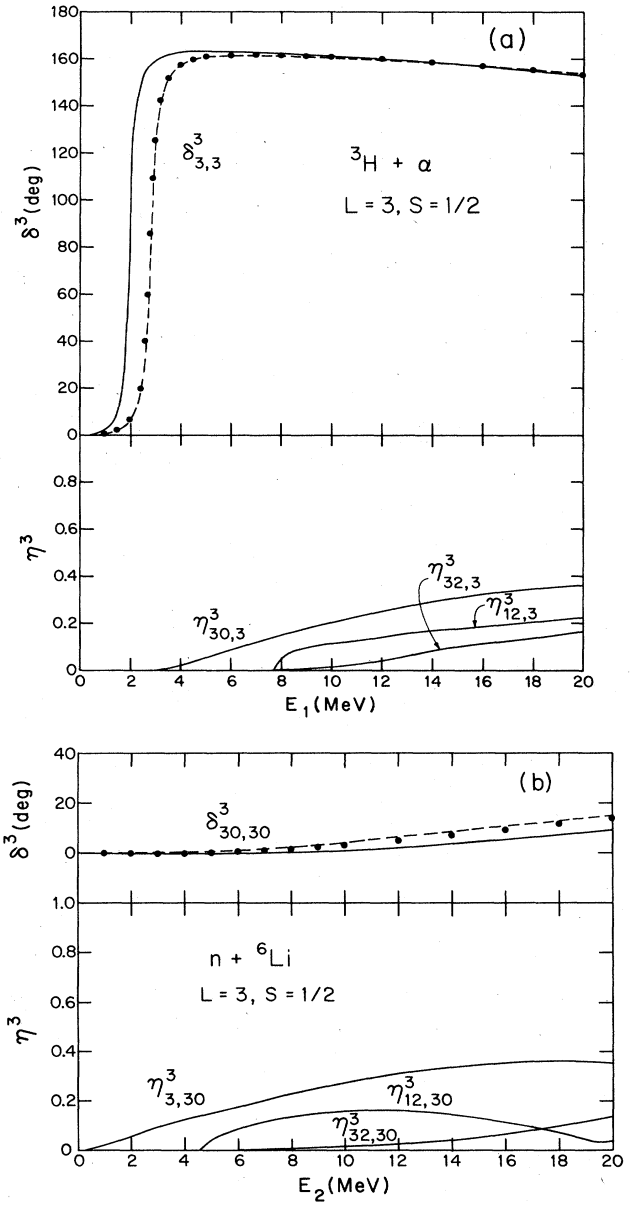

FIG. 9. (a) Same as Fig. 6(a), except that $(L,S)=(3,\frac{1}{2})$. (b) Same as Fig. 6(b), except that $(L,S)=(3,\frac{1}{2})$.

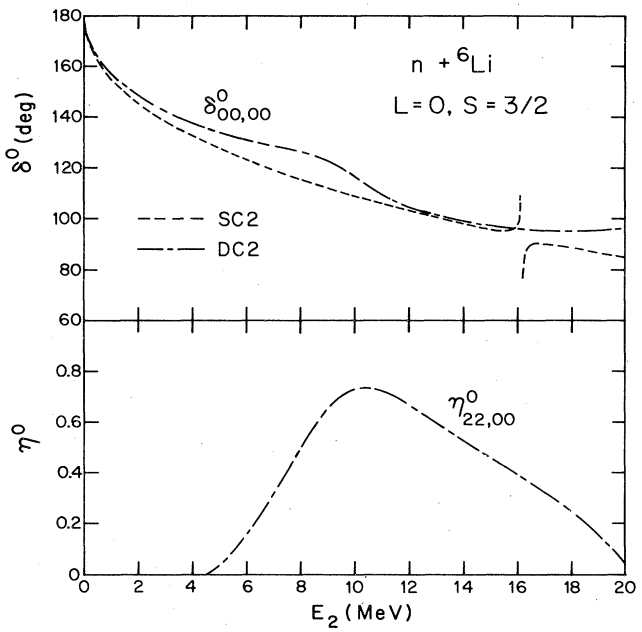

FIG. 10. Calculated phase shifts and transmission coefficients for $(L,S)=(0,\frac{3}{2})$ in the n + ^{6}Li channel. The dashed and dot-dashed curves represent results obtained with SC2 and DC2 calculations, respectively.

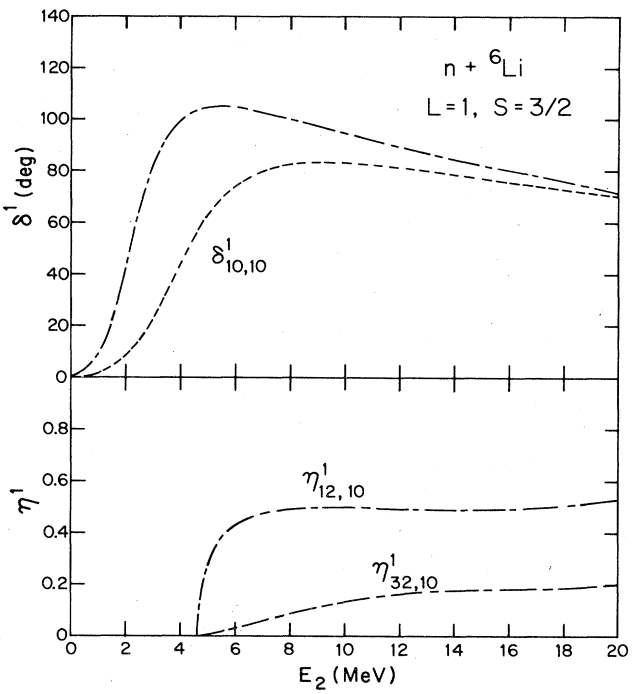

FIG. 11. Same as Fig. 10, except that $(L,S)=(1,\frac{3}{2})$.

tion, the n + ^{6}Li phase-shift curve shows now a dispersionlike resonance behavior around 10.5 MeV. As was mentioned in Sec. II D, this resonance behavior arises as a consequence of rather strong coupling to the n + ^{16}Li*, $l=2$ potential resonance.

The R-matrix study of Knox and Lane[15] requires that a very broad $L=0$, $S=\frac{3}{2}$ state be present in the n + ^{6}Li continuum. In view of our finding here concerning the n + ^{6}Li phase-shift behavior in the low-energy region, we are of the opinion that the postulate of such a positive-parity level is not unreasonable.

The n + ^{6}Li, S-wave scattering length a_+ determined by using low-energy phase-shift values in the DC2 case is 1.99 fm. This value is larger than, but still in reasonable agreement with, the empirical value of 1.15 fm obtained in the R-matrix analysis of Knox and Lane.[15]

2. $L=1$ state (Fig. 11)

Here we see an interesting demonstration of target-clustering and channel-coupling effects. In a single-configuration SM-RGM calculation with ^{6}Li internal function ϕ_5 of FT1, the $(L,S)=(1,\frac{3}{2})$ resonance state occurs at 1.78 MeV. Upon improving the internal function to take proper account of the clustering property of ^{6}Li, our present SC2 calculation shows that this state has now a higher resonance energy of 4.40 MeV (see also the discussion in FT1). By further expanding the model space to include also the n + ^{6}Li* cluster configuration, the DC2 result indicates that the resonance energy becomes smaller and the state is finally located at 2.56 MeV.

Experimentally, there exist $\frac{5}{2}^-$ and $\frac{3}{2}^-$ states at 7.46 and 9.9 MeV, respectively.[34] By averaging the resonance energies of these two states according to spin-orbit weighting, we obtain an empirical value of 1.67 MeV for the $(L,S)=(1,\frac{3}{2})$ state. Comparing with our calculated value of 2.56 MeV, we note that, considering the complexities of this problem, there is indeed a gratifying agreement between theory and experiment.

The importance of centrifugal-barrier effects is again clearly demonstrated here. From Fig. 11, we find that, because of such effects, the transmission coefficient $\eta^1_{12,10}$ is much larger than the transmission coefficient $\eta^1_{32,10}$.

3. $L=2$ state (Fig. 12)

The phase-shift curve in the SC2 case shows that there exists a resonance state at around 10 MeV. This state is, however, so broad that its effects on the n + ^{6}Li cross sections are expected to be quite limited. The situation is changed in the DC2 case. Now, the phase-shift result exhibits a more rapid rise in the low-energy region and indicates the presence of an additional state at 14.5 MeV. This latter state has predominantly a n + ^{6}Li*, $l=2$ cluster structure and expresses itself through a dispersionlike resonance behavior in the n + ^{6}Li phase-shift curve.

The existence of the n + ^{6}Li*, $l=2$ resonance structure overwhelms even the important effects arising from the centrifugal barrier. This is shown in Fig. 12 where one notes that the transmission coefficient $\eta^2_{22,20}$ is even larger than the transmission coefficient $\eta^2_{02,20}$. On the other hand, the barrier effect is still quite evident here, as is seen by the fact that the transmission coefficient $\eta^2_{42,20}$ is small over the whole energy range.

Because of large L and S values in this state, the spin-

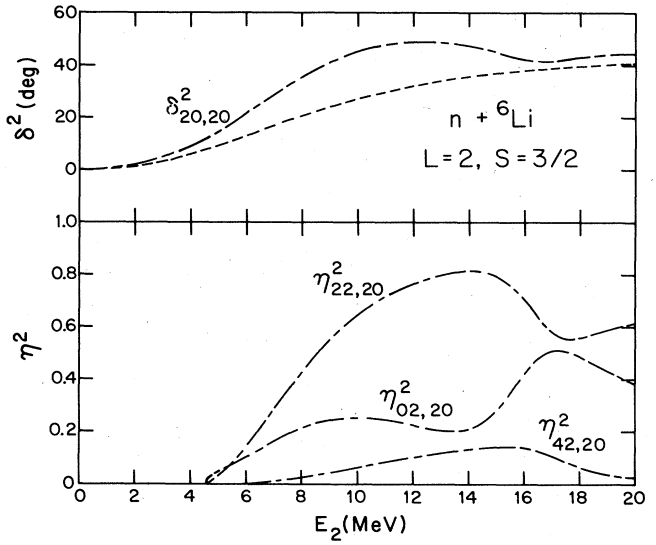

FIG. 12. Same as Fig. 10, except that $(L,S)=(2,\frac{3}{2})$.

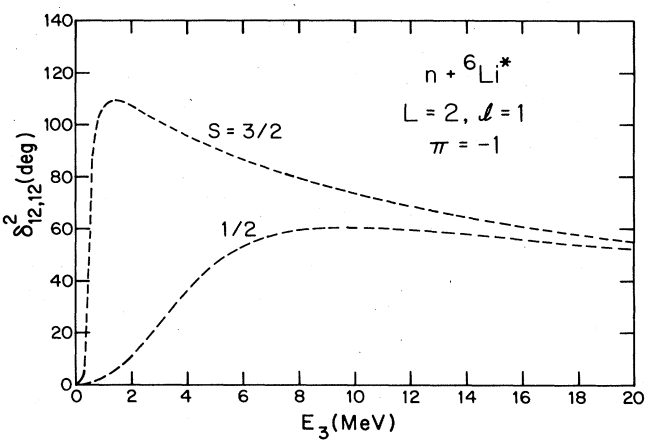

FIG. 13. Calculated n + ^{6}Li* phase shifts $\delta^2_{12,12}$ in $S=\frac{1}{2}$ and $\frac{3}{2}$ states.

orbit contribution will be quite appreciable. With this contribution taken into consideration, one expects that the phase shift in the $\frac{7}{2}^+$ state will, in particular, increase rather rapidly in the low-energy region. Thus, it is likely that low-energy n + ^{6}Li cross sections may be significantly influenced by the presence of such a state (see also the discussion in Ref. 26). It would indeed be interesting to carefully analyze the experimental data to determine whether or not our finding here is borne out.

A phase-shift cusp also exists at the n + ^{6}Li* threshold. This cusp is, however, so small in the present calculation that it cannot be distinctly seen from the phase-shift curve shown in Fig. 12.

4. *L=3 state (not shown)*

The coupling between n + ^{6}Li and n + ^{6}Li* cluster configurations is quite weak. This is evidenced by the small difference of the SC2 and DC2 phase-shift results and the rather small magnitude of the transmission coefficient $\eta^3_{12,30}$ for the dominant n + ^{6}Li* aligned configuration.

E. Unnatural-parity states

Experimentally, there exists in ^{7}Li a $\frac{7}{2}^-$ level with an excitation energy of 9.67 MeV. This level is known to have predominantly an (L,S) value equal to $(2,\frac{3}{2})$. To see whether or not this particular level is permitted in our model space, we have made in the $L=2$ state a single-configuration n + ^{6}Li* calculation consisting of two channels specified by $l=1$ and 3.

In Fig. 13, we show in both $S=\frac{1}{2}$ and $\frac{3}{2}$ states the phase shifts $\delta^2_{12,12}$ as a function of E_3, the relative energy of the neutron and the ^{6}Li* cluster in the c.m. system. The transmission coefficients $\eta^2_{32,12}$ are not shown, since they are rather small in the energy range of interest. As is seen from this figure, there is indeed a prominent $S=\frac{3}{2}$ resonance state at 0.55 MeV above the n + ^{6}Li* threshold. In addition, a broad $S=\frac{1}{2}$ resonance also seems to occur. This latter resonance has, however, a considerably higher excitation energy and lies in an energy region where scant experimental information exists.

The n + ^{6}Li*, $(L,S)=(2,\frac{3}{2})$ configuration can couple with the ^{3}H + α, $(L,S)=(3,\frac{1}{2})$ configuration through the noncentral part of the nucleon-nucleon potential. However, it has been explicitly shown by Hofmann *et al.*[26] that such a coupling mechanism is weak. Instead, they proposed that the coupling between these two configurations is effected through the d + ^{5}He configuration which acts as a doorway structure in this particular situation.

F. Scattering and reaction cross sections

Similar to the finding reported in FT2, one also notes here that, at energies above the n + ^{6}Li* threshold, the calculated cross section σ^*_R for the ^{3}H(α,n)^{6}Li* reaction is generally much larger than the calculated cross section σ_R for the ^{3}H(α,n)^{6}Li reaction. For instance, at $E_1=15.95$ MeV, the calculated ratio σ^*_R/σ_R is 2.79, which agrees quite well with the measured value[32] of 2.53 for the ^{4}He(^{3}He,p) reaction leading to the ground and first excited states of ^{6}Li.

Differential cross sections for ^{3}H + α scattering at $E_1=20$ MeV and for n + ^{6}Li scattering at $E_2=20$ MeV have also been calculated. Here it is found that, as in FT2 and FT3, the main characteristics of the single-configuration results are little affected by the inclusion of other cluster configurations. This is interesting, since it means that, at sufficiently high energies, the essential findings of scattering experiments can already be understood by performing only relatively simple single-configuration calculations.

G. Effects of channel coupling on nucleon-exchange calculations

One of the most interesting findings in single-configuration SM-RGM studies[14,50] is that core-exchange

contributions, arising from antisymmetrization, are very important in nuclear systems where the nucleon-number difference of the interacting clusters is small. As is now well known, these exchange contributions clearly exhibit themselves through a distinct zigzag pattern in the phase-shift result as a function of the relative orbital angular momentum. In this investigation, we wish to determine if the importance of such contributions is significantly modified when channel-coupling effects are included by performing a multiconfiguration calculation utilizing realistic cluster internal functions.

In Fig. 14, we show the L dependence of the $^3\mathrm{H}+\alpha$ phase shift $\delta^L_{L,L}$ at 20 MeV in SC1 and TC cases. For completeness, the reflection coefficient $\eta^L_{L,L}$ is also depicted. From this figure, it is seen that the zigzag patterns are nearly the same in these two calculations. In fact, they are also very similar to the pattern obtained in the SM-RGM case (not shown). This indicates, therefore, that the important characteristics of nucleon-exchange contributions can already be learned by carrying out relatively simple SM-RGM studies, and we are now confident that the general conclusions regarding exchange contributions, summarized in Ref. 50, are valid and can be conveniently used to explain the essential results of many light-ion and heavy-ion scattering experiments, especially at rather high energies.

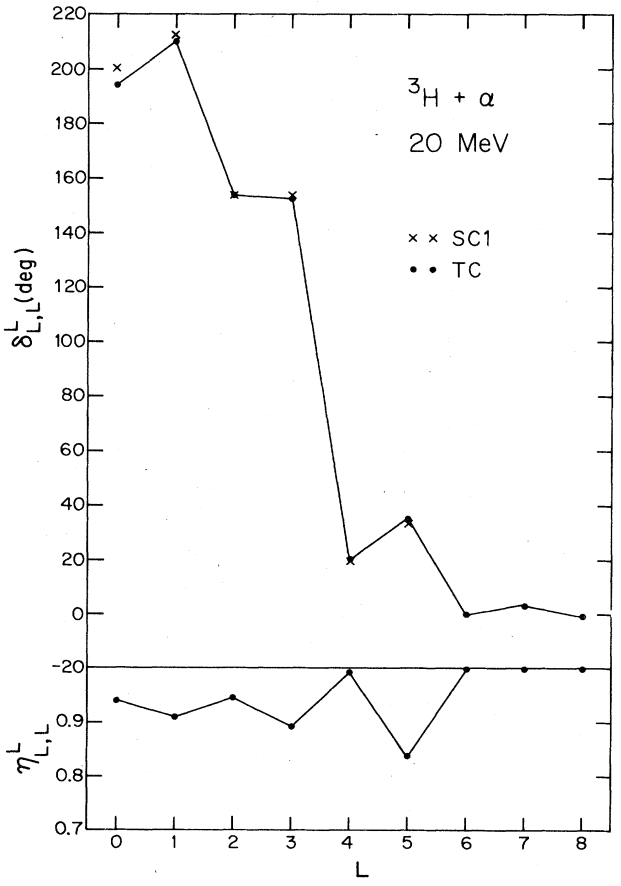

FIG. 14. Comparison of $^3\mathrm{H}+\alpha$ phase shifts at 20 MeV, obtained with SC1 (crosses) and TC (solid circles) calculations. The reflection coefficient in the TC case is also shown.

H. Comparison of calculated and empirical level spectra

Calculated and empirical negative-parity level spectra in the low-excitation region are compared in Fig. 15. In the empirical level spectrum, solid lines represent levels summarized in Ref. 34, while dashed lines represent additional levels obtained from the R-matrix analysis of Ref. 15. For the calculated level spectrum, a Coulomb correction of 0.86 MeV has been made. From this comparison, one finds the gratifying result that, by properly considering the channel-coupling effect and by adopting realistic cluster internal functions, a good agreement between theory and experiment in this complicated seven-nucleon system can be achieved.

We shall not make a similar comparison in the positive-parity case. The $\frac{1}{2}^+$ and $\frac{3}{2}^+$ levels obtained from the R-matrix study[15] are very broad and their energy locations are uncertain by several MeV. In our calculation, the $\mathrm{n}+{}^6\mathrm{Li}$, $(L,S)=(0,\frac{1}{2})$ and $(0,\frac{3}{2})$ phase-shift curves show very flat behavior in the low-energy region. These could be interpreted as indicating the presence of $\frac{1}{2}^+$ and $\frac{3}{2}^+$ levels; however, the level widths will be so large that any precise statement about the positions of these levels would be rather meaningless.

At excitation energies higher than about 12 MeV, our calculation indicates that there may exist broad levels such as the $\frac{7}{2}^+$ level discussed in Sec. III D 3. Experimentally, there is scant information about the level structure in this higher-excitation domain. It would indeed be interesting to carry out further detailed experimental studies and subsequent R-matrix analyses to explore this little-known energy region.

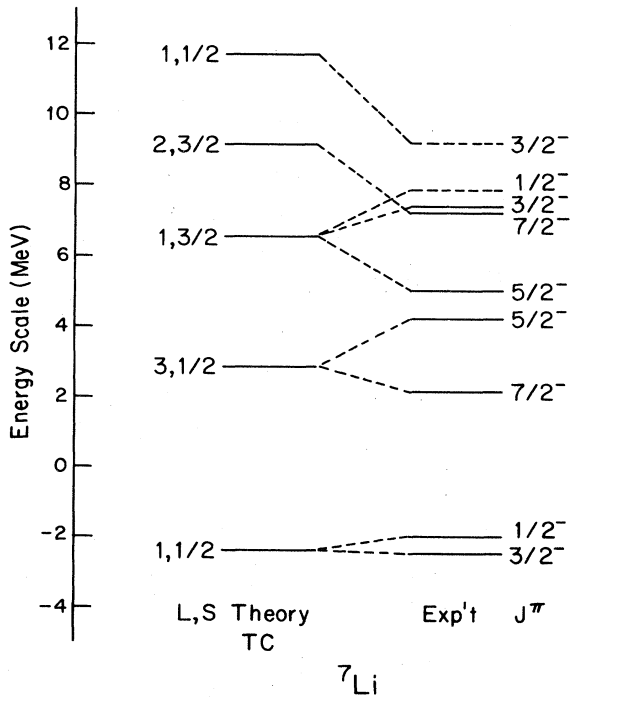

FIG. 15. Comparison of calculated and empirical negative-parity level spectra.

IV. RESULTS OF CALCULATION IN THE QC MODEL SPACE

To make certain that the calculational results reported in the previous section are indeed reasonable, we have made a further study in which the d + ^{5}He cluster configuration is also included. The purpose is of course to see in what way the conclusions reached in Sec. III will be modified by the introduction of this extra freedom. Based on our general understanding that the Pauli principle tends to reduce appreciably the differences between seemingly different cluster structures, our expectation is that such an expansion of the model space may cause some modification in quantitative details, but will not affect the essential characteristics of the results.

As is evident, the adoption of one more cluster configuration will increase greatly the requirement of computational time. Therefore, we shall carry out the examination only in one suitably-chosen L state where the d + ^{5}He configuration is expected to contribute most significantly. The decision as to which L state one should choose is, in fact, not difficult to make. From the discussion given in Sec. III, one sees clearly that, because of centrifugal-barrier effects, channel-coupling contributions become generally rather unimportant when the relative orbital angular momentum l of the cluster configuration under consideration has a large value. Utilizing this information, we can easily decide that the state to be considered should have $L=1$, since only in this L state can the l value in the d + ^{5}He configuration take on the smallest possible value equal to zero. Therefore, we shall conduct our study in the $(L,S)=(1,\frac{1}{2})$ state and compare the QC (four cluster configurations and six channels) results obtained here with the TC (three cluster configurations and four channels) results reported in Sec. III.

First, we shall discuss the ^{3}H + α cluster separation energy in the ground state. With SC1, DC1, TC, and QC calculations, the separation energies are equal to 2.00, 2.85, 3.25, and 3.50 MeV, respectively. Here we see that, as the model space is expanded, the separation energy becomes larger, but the increase in each step does become progressively smaller. The difference between TC and QC results is 0.25 MeV which is much smaller than the difference between SC1 and TC results. This indicates that the addition of the d + ^{5}He cluster configuration has some influence, but the influence is not major.

At this moment, we wish to mention that, by calculating in the SC1 model space and model space similar to the QC space adopted here, Hofmann *et al.*[26] obtained a difference in separation energy equal to about 3 MeV. This value is much larger than the value which we find from this investigation. The reason is that the cluster internal functions employed by these authors do not satis-

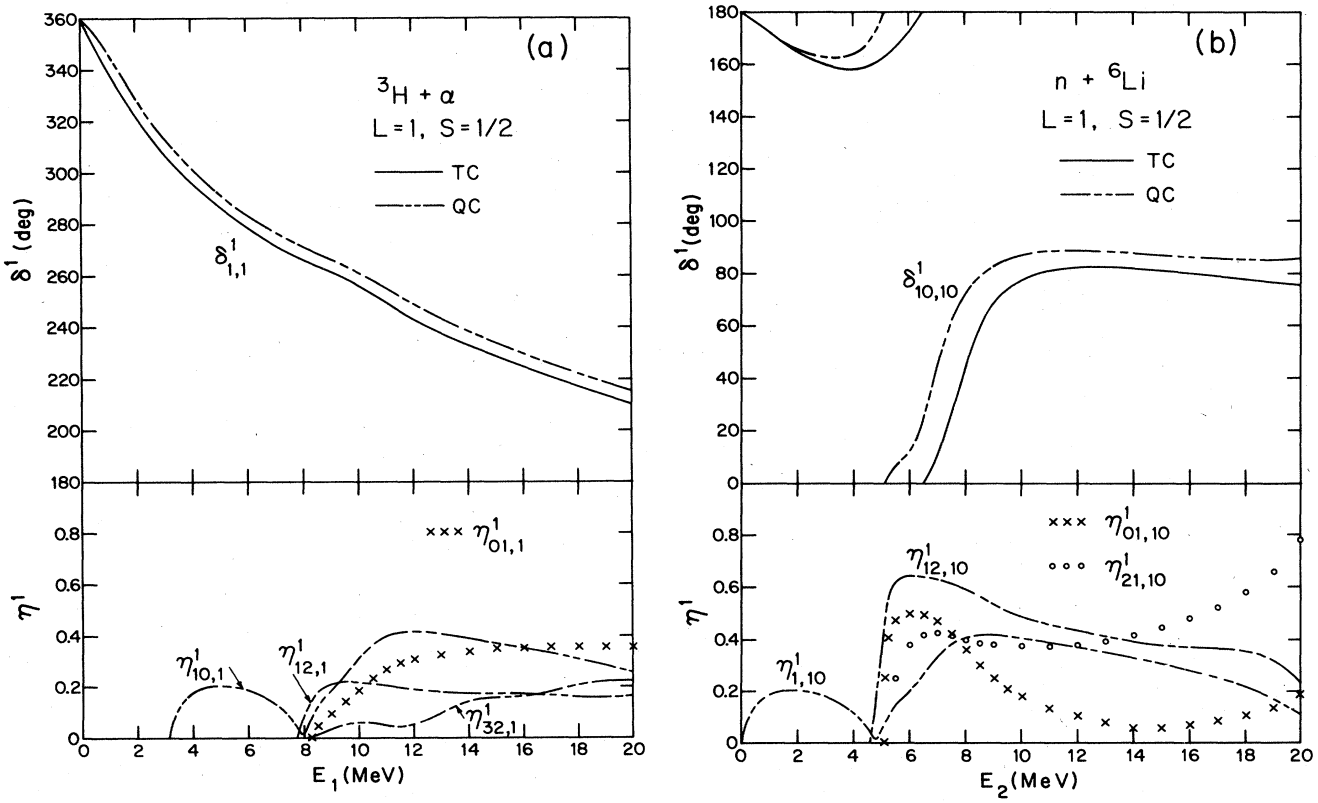

FIG. 16. (a) Comparison of $(L,S)=(1,\frac{1}{2})$, ^{3}H + α phase shifts obtained in the TC (solid curve) and QC (double-dot-dashed curve) cases. The transmission coefficients in the QC case are also shown. (b) Comparison of $(L,S)=(1,\frac{1}{2})$, n + ^{6}Li phase shifts obtained in the TC (solid curve) and QC (double-dot-dashed curve) cases. The transmission coefficients in the QC case are also shown.

fy the variational stability condition stressed in Sec. II B and, hence, an expansion of the model space serves in their case the dual role of not only representing channel-coupling effects, but also making an unrealistic correction of the internal structures of the interacting clusters.

A comparison between TC (solid curves) and QC (double-dot-dashed curves) phase-shift results is shown in Figs. 16(a) and (b). In addition, various transmission coefficients are also depicted.[51] From these figures, one notes that the phase-shift features obtained in these two calculations are qualitatively very similar. Even the quantitative difference is seen to be rather moderate. With the addition of the $d + {}^5He$ configuration, the $(L,S)=(1,\frac{1}{2})$ resonance is lowered by about 1 MeV and there appears a slightly wavy behavior in the $n + {}^6Li$ phase-shift curve around E_2 equal to 6 MeV. This wavy behavior signifies the presence of a state which has predominantly a $d + {}^5He$ cluster structure. However, because of rather weak coupling, the influence of this state on $n + {}^6Li$ scattering properties is quite minimal.

In summary, we feel that the reduction effect of the Pauli principle is demonstrated in this study. The utilization of the QC model space is required for a detailed, quantitative examination, but is not essential to understand the basic characteristics of the seven-nucleon system.

V. CONCLUSION

In this investigation, the properties of the seven-nucleon system are examined with a multiconfiguration and multichannel RGM study. The model space adopted for most of the calculations is spanned by the $^3H + \alpha$, $n + {}^6Li$, and $n + {}^6Li^*$ cluster configurations. However, in one carefully-selected orbital angular momentum state, we have also performed a calculation by further including the $d + {}^5He$ cluster configuration in order to make certain the reliability of the conclusions.

The effect of the Pauli principle in reducing the differences between seemingly different cluster structures is rather well demonstrated. The addition of the $d + {}^5He$ cluster configuration has some moderate influence, but does not affect the basic characteristics of the results.

The main improvement in this investigation, over a previous multiconfiguration RGM study,[20] is the adoption of realistic cluster internal functions which explain the form-factor data in a large q^2 range and which satisfies quite well the variational stability condition. Such an improvement requires the complicated, analytical formulation for a three-cluster system, which we achieved[22] by carefully classifying the nucleon-exchange terms and by making extensive use of the techniques of integral transform.

The specific distortion of the $^3H + \alpha$ system turns out to be quite significant. With our multiconfiguration calculation, we find that the ground-state energy is improved by more than 1 MeV. This improvement is substantially larger than that found in Ref. 24, where only radial distortion effects were taken into consideration.

The calculated level spectrum agrees well with the level spectrum empirically determined. The energy positions of both natural-parity and unnatural-parity levels are reasonably explained. In addition, the calculation predicts the existence of broad levels in the higher-excitation region. These predictions should be helpful in future phenomenological analyses, when good-quality higher-energy data become available.

Our interesting finding should be emphasized here. Because of centrifugal-barrier effects, the aligned configuration is found to be particularly important. This is useful information to have, since it will enable one to simplify the calculation by adopting a smaller number of channels. As is evident, such a simplification would certainly have to be made in future considerations of more complicated systems, since one of the major problems facing a multiconfiguration calculation is connected with severe computational requirements.

At sufficiently high energies where sharp resonance levels of the compound system do not exist, this investigation shows that the main characteristics of scattering cross sections and the essential properties of nucleon-exchange terms can already be learned by performing relatively simple single-configuration calculations. Again, this is a gratifying finding, since it means that one can now employ the RGM to systematically explain the experimental data of light-ion and heavy-ion scattering in the higher-energy region.[52]

In conclusion, we feel that, with the completion of this investigation, we have achieved a sufficient understanding of the interesting properties of the seven-nucleon system. Additionally, we have learned how to make various simplifications in future calculations. This is important, since with such knowledge we can now proceed to study other more complicated problems and hope to comprehend eventually the intricate nature of three-cluster interaction.

This research was supported in part by the U.S. Department of Energy under Contract No. DOE/DE-AC02-79 ER 10364.

[1]J. A. Wheeler, Phys. Rev. **52**, 1083 (1937); **52**, 1107 (1937).
[2]K. Wildermuth and Y. C. Tang, *A Unified Theory of the Nucleus* (Vieweg, Braunschweig, 1977).
[3]Y. C. Tang, M. LeMere, and D. R. Thompson, Phys. Rep. **47**, 167 (1978).
[4]Y. C. Tang, *Microscopic Description of the Nuclear Cluster Theory,* in *Lecture Notes in Physics,* Vol. 145 (Springer, Berlin, 1981), and references contained therein.
[5]K. Ikeda *et al.*, Prog. Theor. Phys. Suppl. **68**, 1 (1980).
[6]T. Ando, K. Ikeda, and A. Tohsaki-Suzuki, Prog. Theor. Phys. **64**, 1608 (1980).
[7]H. Schultheis and R. Schultheis, Phys. Rev. C **25**, 2126 (1982).
[8]Both calculations (Refs. 6 and 7) use the nucleon-nucleon potential B1 of D. M. Brink and E. Boeker, Nucl. Phys. **A91**, 1

(1967).

[9]H. H. Hackenbroich, in *Proceedings of the Second International Conference on Clustering Phenomena in Nuclei, College Park, Maryland, 1975,* edited by D. A. Goldberg, J. B. Marion, and S. J. Wallace (National Technical Information Service, Springfield, Virginia, 1975), p. 107.

[10]H. H. Hackenbroich, in *Proceedings of the Fourth International Symposium on Polarization Phenomena in Nuclear Reactions, Zurich, 1975,* edited by W. Grüebler and V. König (Birkhaüser, Basel, 1976), p. 133.

[11]W. Schütte, H. H. Hackenbroich, H. Stöwe, P. Heiss, and H. Aulenkamp, Phys. Lett. **65B**, 214 (1976).

[12]H. Hutzelmeyer, Ph.D. thesis, Florida State University, 1968.

[13]H. H. Hackenbroich, in *Proceedings of the International Symposium on the Present Status and Novel Developments in the Nuclear Many-Body Problem, Rome, 1972,* edited by F. Galogero and C. C. Degli Atti (Editrice Compositori, Bologna, 1973).

[14]See, e.g., M. LeMere, D. J. Stubeda, H. Horiuchi, and Y. C. Tang, Nucl. Phys. **A320**, 449 (1979).

[15]H. D. Knox and R. O. Lane, Nucl. Phys. **A403**, 205 (1983).

[16]J. N. Bahcall, W. F. Huebner, S. H. Lubow, P. D. Parker, and R. K. Ulrich, Rev. Mod. Phys. **54**, 767 (1982).

[17]A. S. Divatia, in *Proceedings of the Seventh International Conference on Few-Body Problems in Nuclear and Particle Physics, Delhi, 1975—76,* edited by A. N. Mitra, I. Slans, V. S. Bhasin, and V. K. Gupta (North-Holland, Amsterdam, 1976), p. 469.

[18]H. H. Hackenbroich and T. H. Seligman, Phys. Lett. **41B**, 102 (1972).

[19]Y. Fujiwara and Y. C. Tang, Phys. Rev. C **27**, 2457 (1983).

[20]Y. Fujiwara and Y. C. Tang, Phys. Rev. C **28**, 1869 (1983).

[21]Y. Fujiwara and Y. C. Tang, Phys. Rev. C **29**, 2025 (1984).

[22]For a system consisting of an α cluster and two s-shell clusters, the general formulation of a three-cluster RGM, based on the coupled-channel formalism, is given by Y. Fujiwara and Y. C. Tang, University of Minnesota Report UM-RGM2, 1984.

[23]R. Beck, R. Krivec, and M. V. Mihailović, Nucl. Phys. **A363**, 365 (1981).

[24]H. Kanada, T. Kaneko, and Y. C. Tang, Nucl. Phys. **A380**, 87 (1982).

[25]The calculation of T. Kajino, T. Matsuse, and A. Arima, Nucl. Phys. **A414**, 185 (1984), is very similar to that of Kanada *et al.* discussed in Ref. 24.

[26]H. M. Hofmann, T. Mertelmeier, and W. Zahn, Nucl. Phys. **A410**, 208 (1983).

[27]H. Eikemeier and H. H. Hackenbroich, Nucl. Phys. **A169**, 407 (1971).

[28]M. Kamimura, Prog. Theor. Phys. Suppl. **62**, 236 (1977).

[29]T. H. Seligman and W. Zahn, J. Phys. G **2**, 79 (1976); H. Horiuchi, Prog. Theor. Phys. **55**, 1448 (1976).

[30]This restriction is, in fact, not too severe, since the properties of the subsystems can still be well accounted for by the choice of appropriate relative-motion functions.

[31]J. A. Koepke, R. E. Brown, Y. C. Tang, and D. R. Thompson, Phys. Rev. C **9**, 823 (1974).

[32]J. A. Koepke and R. E. Brown, Phys. Rev. C **16**, 18 (1977).

[33]In this section, the discussion deals with natural-parity states, i.e., states with $\pi=(-1)^L$.

[34]F. Ajzenberg-Selove, Nucl. Phys. **A413**, 1 (1984).

[35]D. R. Thompson, M. LeMere, and Y. C. Tang, Nucl. Phys. **A286**, 53 (1977).

[36]Y. Fujiwara, Y. C. Tang, and H. Horiuchi, J. Math. Phys. **25**, 2826 (1984).

[37]For this comparison, the calculated body form factors $F_B(^3\text{He})$ and $F_B(^3\text{H})$ are assumed to be the same.

[38]M. LeMere, R. E. Brown, Y. C. Tang, and D. R. Thompson, Phys. Rev. C **12**, 1140 (1975); see also, D. R. Thompson, Y. C. Tang, and F. S. Chwieroth, *ibid.* **10**, 987 (1974).

[39]T. Kajino, T. Matsuse, and A. Arima, Nucl. Phys. **A413**, 323 (1984).

[40]Y. C. Tang, K. Wildermuth, and L. D. Pearlstein, Nucl. Phys. **32**, 504 (1962); V. G. Neudatchin and Yu. F. Smirnov, Prog. Nucl. Phys. **10**, 275 (1969).

[41]H. J. Mang, Annu. Rev. Nucl. Sci. **14**, 1 (1964); D. Kurath, Phys. Rev. C **7**, 1390 (1973); M. Ichimura, A. Arima, E. C. Halbert, and T. Terasawa, Nucl. Phys. **A204**, 225 (1973). A better, but slightly more complicated, definition for this amplitude has been introduced by T. Fliessbach, Z. Phys. A **272**, 39 (1975). [For an interesting application of this definition in ^{6}Li and ^{7}Be, see H. Walliser and Y. C. Tang, Phys. Lett. **135B**, 344 (1984).] We have not adopted this latter definition here, simply because we are merely interested in a qualitative understanding of the clustering properties of the nuclei involved.

[42]It should be noted that the $n+{}^6\text{Li}$, $n+{}^6\text{Li}^*$, and $d+{}^5\text{He}$ cluster configurations are uniquely specified by the value of I, equal to 0, 2, and 1, respectively.

[43]S. Saito, S. Okai, R. Tamagaki, and M. Yasuno, Prog. Theor. Phys. **50**, 1561 (1973).

[44]Y. Fujiwara and Y. C. Tang, Phys. Lett. **131B**, 261 (1983).

[45]Steplike resonances will frequently be plotted as breaks in the phase-shift curves.

[46]H. Walliser and T. Fliessbach, Nucl. Phys. **A394**, 387 (1983).

[47]This is the main reason why we prefer to call it Pauli resonance instead of the almost-forbidden state. With the latter, one might get the erroneous impression that, even within the chosen model space, it has a spurious character and, therefore, is undesirable.

[48]F. S. Chwieroth, Y. C. Tang, and D. R. Thompson, Phys. Lett. **46B**, 301 (1973). It should be mentioned that the procedure of introducing an imaginary potential to crudely simulate the presence of additional reaction channels is actually not within the proper framework of the RGM.

[49]E. P. Wigner, Phys. Rev. **73**, 1002 (1948); L. D. Landau and E. M. Lifshitz, *Quantum Mechanics,* 3rd ed. (Pergamon, Oxford, 1977).

[50]M. LeMere, Y. Fujiwara, Y. C. Tang, and Q. K. K. Liu, Phys. Rev. C **26**, 1847 (1982); Y. C. Tang, in *Proceedings of the International Symposium on Clustering Phenomena in Nuclei, Tübingen, 1981,* edited by P. Kramer and R. Schultheis (Attempto, Tübingen, 1981).

[51]For clarity in presentation, we have not plotted any transmission coefficient which has a value smaller than 0.15 in the whole energy range considered.

[52]It should be mentioned that, from the viewpoint of simplicity in data analyses, scattering experiments should best be performed at energies higher than about 25 MeV/nucleon. The reason is that, at such energies, nucleon-exchange terms can be conveniently classified into class-A and class-B terms which make their dominant contributions in different angular regions (see Ref. 50).